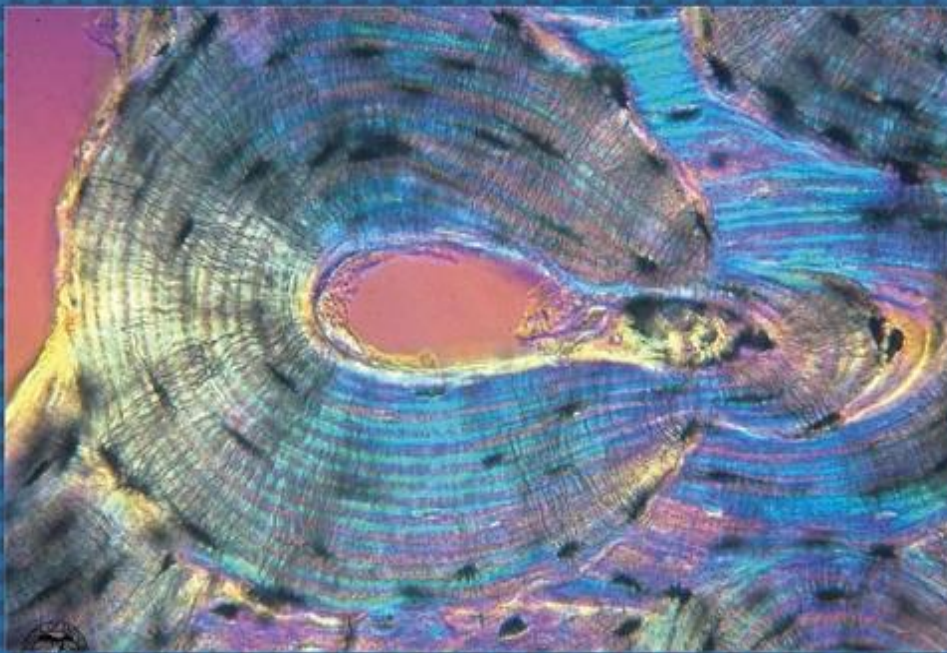




EGYPTIAN ACADEMIC JOURNAL OF
BIOLOGICAL SCIENCES
HISTOLOGY & HISTOCHEMISTRY

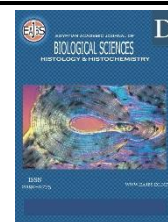
D



ISSN
2090-0775

WWW.EAJBS.EG.NET

Vol. 16 No. 1 (2024)



Can Neonatal Maternal Separation Affect the Morphometric Parameters and Ultrastructure of Sertoli Cells and Spermatogenic Cells in Rat Testis Via Modulation of Hypothalamic-Pituitary-Thyroid/Adrenal and Gonadal axes?

Walaa Adel Abdelmoez

Department of Anatomy and Embryology, Faculty of Medicine, Ain-Shams University, Abbassia, Postal code: 11591 .Cairo, Egypt.

*E-mail: walaa_adel@med.asu.edu.eg

ARTICLE INFO

Article History

Received:5/1/2024

Accepted:7/2/2024

Available:11/2/2024

Keywords:

Maternal Separation;
Hypothalamic;
Pituitary; Sertoli cells;
Spermatogenic cells.

ABSTRACT

Neonatal maternal separation is used to evaluate the effects of early life stress on various systems. The current study evaluated the impact of early life stress exposure on the morphometry and ultrastructure of adult male albino rat testis and clarified its intimate relation with hypothalamic-pituitary-thyroid/Adrenal and gonadal axes. Thirty pregnant rats (dams) were divided into groups (i), (ii) and (iii). Neonates(pups) were also divided into; control (I), and neonatal maternal separation II (NMS II): pups were segregated from their dams for 2 hours /day. Group (NMSIII): pups were segregated from their dams for 4 hours/day from postnatal day 0 to postnatal day 14. Histological results revealed distortion affecting the testicular parenchyma in groups (II) and (III). Sections from both groups revealed markedly disrupted seminiferous tubules; decreased height of germinal epithelium; and decreased tubular diameter with widened interstitium. Immunohistochemical results revealed that the number of proliferating cells (ki67 positive cells) and inducible nitric oxide synthetase (iNOS positive cells) were significantly attenuated in both groups II, III. No substantial change was observed in the quantity of apoptotic cells. Degenerative signs were observed by transmission electron microscopy in both groups II and III; but much more extensive in group III. Sertoli cells, spermatogonia and primary spermatocytes showed irregular nuclear membrane, degenerated mitochondria with distorted crista, dilated endoplasmic reticulum and rarified cytoplasm. Extensive drop in sperm density in epididymal tissue was clearly observed in group III. Biochemical analysis revealed increased serum levels of oxidative stress markers and significant attenuation of different hormones of the Hypothalamic-Pituitary axis in groups II and III.

INTRODUCTION

It has been proved that exposure to early-life stress disrupts the normal growth of neonates, resulting in a variety of negative health outcomes (Császár-Nagy & Bókkon, 2018). The neonatal-maternal separation (NMS) model is applied to evaluate the deleterious effects of stress on neonates. It may lead to psycho-developmental and neurodevelopmental disorders, such as anxiety-like behavior (Khan *et al.*,2023).

Moreover, (NMS) has become one of the most extensively used experimental models to study the alterations at the endocrine and behavioral levels in rodents as a result of early-life stress exposure (Bodensteiner *et al.*,2014). Previous studies have examined the effects of various types of stress on sex hormones and researchers are still attempting to comprehend the mechanisms by which stress influences the reproductive functions of both sexes (Hodes & Krop, 2023).

The three divisions of the hypothalamic-pituitary-gonadal axis (HPG axis) contain stress-related hormones that can affect sexual function (Thumfart *et al.*, 2022). Conversely, it is widely recognized that adrenal corticosteroids, adrenocorticotropic hormone (ACTH), and corticotropin-releasing factor (CRF) have a pivotal role in regulating the impact of stress on reproductive functions (Kilic *et al.*, 2021). Although numerous studies have provided evidence of the harmful impacts of NMS on various organs in both humans and animals, the exact mechanisms through which NMS induces these health effects are still not fully clarified (Crombie *et al.*, 2021).

The impact of various factors, including prenatal and neonatal exposure to chemicals and nutrients, on the male reproductive system is well documented. Mutations in gene expression levels and morphological abnormalities have been associated with male reproductive development (Eskandari *et al.*, 2023). Concerning the male reproductive system dysfunction induced by NMS, maternal segregation of rodents has been related in multiple studies to a reduction in testicular weight and serum testosterone level. These investigations, however, were devoid of histological evaluations (Gonsioroski *et al.*, 2020). Moreover, the present study hypothesized that the separation of neonates away from their mothers could affect the ultrastructure and function of Sertoli cells and spermatogenic cells in male albino rats' testis via increased oxidative stress condition and disturbance of different hormones of Hypothalamic-Pituitary axis. So, histological and immunohistochemical analyses are thus incorporated into the current work to investigate the impacts of NMS on male reproductive organs.

MATERIALS AND METHODS

Experimental Design & Procedures:

15 adult male and 15 adult female albino rats were included in the current study weighing between 150 and

200 g each. They were confined in stainless steel cages measuring 30x35cm, two rats/cage. The study excluded rats with a disease, had walking problems, bad fur and rats that had been used in previous experiments. Rodents were exposed to 12 hours light/dark cycle and allowed daily diet ad libitum and free water access and housed in an environment with suitable ventilation. Following one week of acclimatization, animals were mated. Upon detection of copulation plugs, males and females were segregated.

Maternal Separation Model:

Pregnant rats (dams) were divided into 3 groups; 5 mothers/each: control group (i), maternal separation group (ii) and maternal separation group (iii). Rats were provided with a suitable environment, adequate ventilation and allowed daily diet ad libitum and free water access till the day of birth (day 0). At the date of birth, neonates were also subdivided into three different groups:

Control group(I): After birth; neonates included in this group were weighed only. Pups were kept with their dams in the same cage (no separation).

Neonatal Maternal Separation group (NMS II): After birth; neonates included in this group were isolated from their dams for 2 h/day, from postnatal day (PND) 1 to 14.

Neonatal Maternal Separation group (NMS III): After birth; neonates included in this group were isolated from their dams for 4 h/day, from postnatal day (PND) 1 to 14.

Each dam was relocated from her original cage to an alternative one. The pups remained at room temperature in their home cages. Water and standard food were supplied for each dam. Once the separation period had ended, every dam was returned to its original cage. All neonates were weighed daily (from day 1 to day 14) for average weight gain estimation. At the end of the experimental period (ten weeks' duration); the rodents were administered ketamine (90 mg/kg) + xylazine (15 mg/kg) intraperitoneally to be anesthetized (Kilic *et al.*, 2021); then

they were subsequently sacrificed. Testis Samples were collected for histopathological and immunohistochemical analysis (Kageyama *et al.*,2021).

Histological and Immunohistochemical Techniques:

For Light Microscopy:

Testis samples were dissected, quickly fixed for ten days in 10% neutral formalin and processed into paraffin blocks. Sections of 5 to 7 μm thickness were cut and stained with hematoxylin and eosin stain (H&E) (Bancroft & Gamble,2008). Other specimens were rinsed for two hours in phosphate buffer and then the specimens were prepared for semithin sections. Semithin sections of one-micron thickness were cut and stained with a 1% concentration of toluidine blue. The stained sections were investigated using an Olympus light microscope equipped with an automatic photomicrographic camera system (Suvarna *et al.*,2018).

For Immunohistochemistry:

Terminal Deoxynucleotidyl Transferase dUTP Nick End Labeling (TUNEL) Assay:

To investigate the apoptosis, DNA end labelling in situ was applied. Following deparaffinization and hydration, sections were subjected to proteinase K treatment. In order to suppress endogenous peroxidase, the sections were preserved in a solution containing 3% hydrogen peroxidase solutions. As instructed by the manufacturer, sections were stained with 3,3-diaminobenzidine (DAB) chromogen solution until a color reaction was observed under a microscope. A counterstain in the form of Mayer's hematoxylin was applied. TUNEL-positive cells displayed in the sections the same morphological and staining characteristics as the positive control (Duan *et al.*,2003).

Immunohistochemical Analysis of iNOS and Ki-67:

To perform immunostaining, serial sections of paraffin blocks measuring 5 μm in thickness were

adhered to glass transparencies and incubated at 65° C for an entire night. Following a 1–2-minute deparaffinization in xylene, the sections were rehydrated in ethanol for 3 minutes and distilled water for 5 minutes. By applying 0.3% hydrogen peroxide for ten minutes at ambient temperature. Inhibition of endogenous peroxidase activity was observed. Following a thorough rinsing in phosphate-buffered saline (PBS), non-specific binding was impeded by incubating the sample in 5% normal goat serum overnight at room temperature. Sections were subsequently incubated with 1:100 of primary antibody per section; iNOS (Catalogue #PA5-17106; 100 L) ThermoFisher scientific. Anti-Ki-67 (rabbit polyclonal antibody, sc-15402, 1:200) ThermoFisher Scientific, United States of America. Following a PBS rinse of twenty minutes, sections were incubated with a secondary antibody that had been biotinylated. The sections were treated with a solution containing the enzyme conjugate "Streptavidin–Horseradish peroxidase" after a duration of 10 minutes. In order to observe the binding of the secondary antibody, 0.03% H₂O₂ was added to 3,3-diaminobenzoic acid (DAB) that had been dissolved in PBS prior use. Hematoxylin was utilized as a counterstain (Khodamoradi *et al.*,2020).

For Electron Microscopy:

In accordance with the standard protocols; rodent testis and epididymis samples were prepared for transmission electron microscopy. After fixation in 2.5% phosphate-buffered glutaraldehyde at 4°C for two hours, samples were cleansed in phosphate-buffered saline. Specimens were then fixed for one hour at 4°C in 1% phosphate buffer osmium tetroxide. Samples were dehydrated in ascending alcohol concentrations, submerged in propylene oxide and encapsulated with an epoxy resin mixture. Using a light microscope L/M, semithin sections were examined to identify the appropriate regions. Uranyl acetate and lead citrate were used as contrast agents to examine ultrathin sections (80-90nm

thick). The slices were observed with a transmission electron microscope (TEM) ("Jeol" E.M-100 CX11; Japan) at Ain Shams University's electron microscopy laboratory (Kue,2007).

For Biochemical Analysis:

Blood samples were centrifuged at 4,000 rounds per minute after coagulation for ten minutes. Hypothesis testing was conducted on serum samples to determine the concentration of hormones using enzyme-linked immunosorbent assay (ELISA). Following the addition of the attenuated serum sample to the capture antibody-coated ELISA plate, the plate was incubated for a predetermined amount of time. Following the removal of the unbound sample by rinsing, the detection antibody was introduced onto the plate. Substrate was introduced subsequent to incubation and rinsing, absorbance was measured on a spectrophotometer (ELx 800; Bio-Tek Instruments Inc., Winooski, VT, USA) utilizing a microplate reader. The collected serum was analyzed for rat FSH and LH concentrations using ELISA Kits (cat no: ER0960, Fine Biotech, Wuhan, Hubei, China; cat no: ER1123; and rat testosterone using Rat Testosterone ELISA Kit, cat no: EH1642, Fine Biotech, Wuhan, Hubei, China). Rat serum TSH estimation was performed using an ELISA Kit (catalogue number: ER1411, Fine Biotech, Wuhan, Hubei, China). Rat serum T3 and ACTH (ELISA Kits, cat no. ER1720 and ER0382, respectively; Fine Biotech, Wuhan, Hubei, China); and free rat serum Cortisol (ELISA Kit, cat no. ER1651. Fine Biotech, Wuhan, Hubei, China). Oxidative stress markers, including malondialdehyde dehydrogenase (MDA) and superoxide dismutase (SOD), were quantified in order to assess the oxidative stress state. ELISA assays E-BC-K025-S (Elabscience Biotechnology, USA) and E-BC-K020 were utilized for this purpose.

Morphometric Analysis:

Histology and Cell Biology Department of Faculty of Medicine; Ain Shams University performed

measurements using the image analyzer. The area percentage of immunological staining was determined using seven fields from seven independent serial sections obtained from seven animals in each group. The expression of TUNEL, iNOS, and ki67 was quantified by determining the percentage of positively stained regions relative to the total area of testicular tissue. Estimates were made regarding the height of germinal epithelium and the diameter of seminiferous tubules.

Statistical Analysis:

Data were collected and presented as mean and standard deviation. Version 23 of SPSS was applied to the data analysis. The Bonferroni post hoc test was employed in conjunction with a one-way analysis of variance (ANOVA) to ascertain the significance of differences between groups. Assuming a P-value below 0.05, the result is considered statistically significant (Sawilowsky,2005).

RESULTS

Histopathological Results:

Examining sections of the control group (I) stained with H&E and toluidine blue; revealed the general architecture of testicular parenchyma consisting of multiple well-arranged seminiferous tubules with regular circular outlines and narrow lumen. The tubules are connected by thin interstitial gaps containing Leydig cells with their associated blood vessels and filled with loose areolar tissue (Fig.1A,2A). Moreover, the germinal epithelium appeared consisting of sertoli cells with pale acidophilic cytoplasm and resting on the basement membrane, spermatogonia with deeply stained nuclei and primary spermatocytes with large size and vesicular nuclei. The secondary spermatocyte appeared smaller in size (Fig.1B). All germ cell layers exhibited active mitotic figures and multiple nucleoli (Fig.2B).

Furthermore, examination of sections from group II showed distortion of the normal architecture of testicular parenchyma; the seminiferous tubules

appeared with abnormal tubular shape, irregular outline; narrow lumen and sloughed germ cells inside their lumen with widened interstitium (Fig.1C,2C). With higher magnification; the thickness of the germ cell layer was apparently decreased with decreased signs of active mitosis (Figs.1D,2D). In addition, sections obtained from group III showed extensive distortion in the shape of seminiferous tubules. They

appeared with widened lumen and sloughed germ cells obliterating their lumen. The interstitial cells showed signs of degeneration with extensively widened interstitium (Figs.1E,2E). The higher magnification showed an extensive decrease in the thickness of germ cell layers and irregular shape of Sertoli cells, decreased mitotic figures with marked thinning of the basement membrane (Figs.1F,2F).

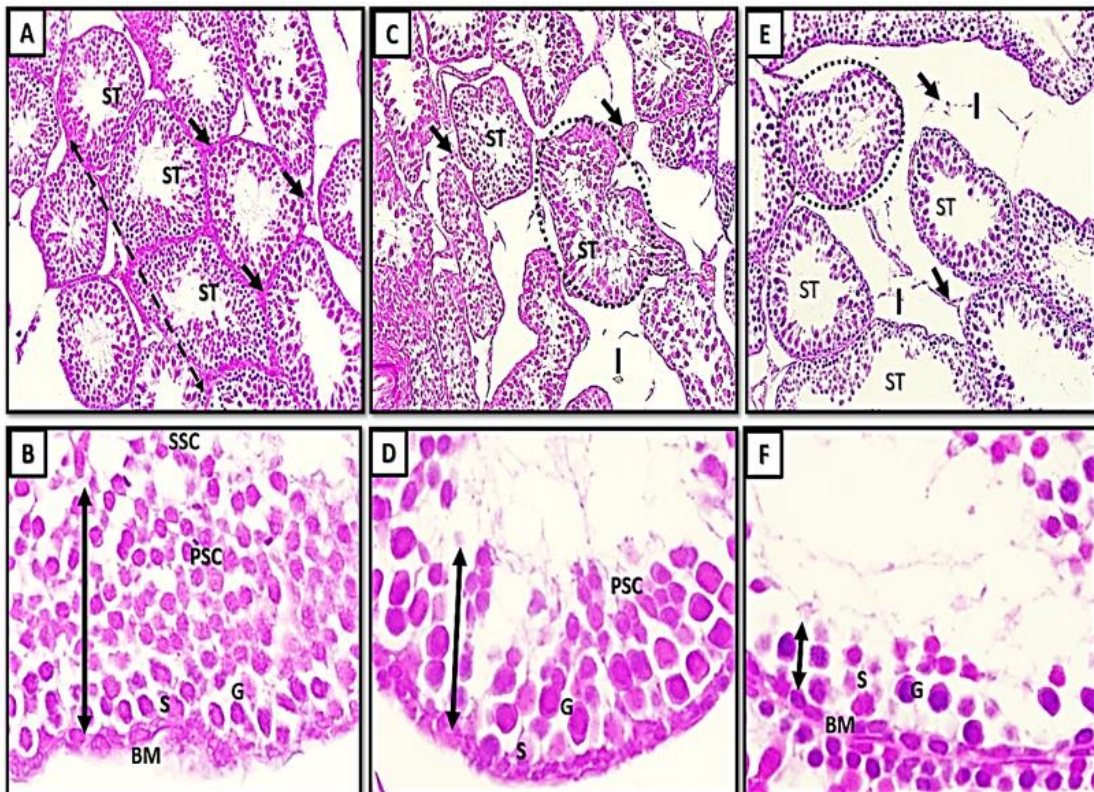


Fig.1A: A transverse section of rat testis from (group I) showing the testicular parenchyma made up of multiple seminiferous tubules (ST) with nearly circular outline and narrow lumen. The tubules connected by thin interstitial gaps containing the leydig cells, their associated blood vessels (black arrows) and filled with loose areolar tissue. Note, the regular arrangement of seminiferous tubules (double head dotted arrow) (X200). The higher magnification in **Fig.1B:** showing full thickness of germinal epithelium (double head arrow). Sertoli cells(S) appears with acidophilic cytoplasm and resting on the basement membrane (BM). Spermatogonia (G) with their deeply stained nuclei and pale cytoplasm. Primary spermatocytes (PSC) with large size and vesicular nuclei and secondary spermatocyte (SSC) appears smaller in size(X1000). **Fig.1C:** showing distorted architecture of testicular parenchyma; the seminiferous tubules (ST) appear with irregular outline; narrow lumen and sloughed germ cells inside their lumen (encircled tubule) and widened interstitium(I). Note also the decreased number of leydig cells (black arrows) (x200). With higher magnification(fig.1D) showing different cellular components of the germinal epithelium Sertoli cells(S), Spermatogonia (S) and primary spermatocytes (PSC) but with decreased thickness of germ cell layer (double head arrow) (X1000). **Fig.1E:** showing extensive distortion in the shape and arrangement of seminiferous tubules (ST) with widened lumen and sloughed germ cells inside their lumen. The interstitial cells are markedly degenerated (black arrows) with extensively widened interstitium(I)(X200). The higher magnification showing extensive decrease in the thickness of germ cell layers (double head arrow) and irregular shape of Sertoli cell(S), decreased number of Spermatogonia (G) with marked thinning of the basement membrane(BM)(X1000). (H&E Stain).

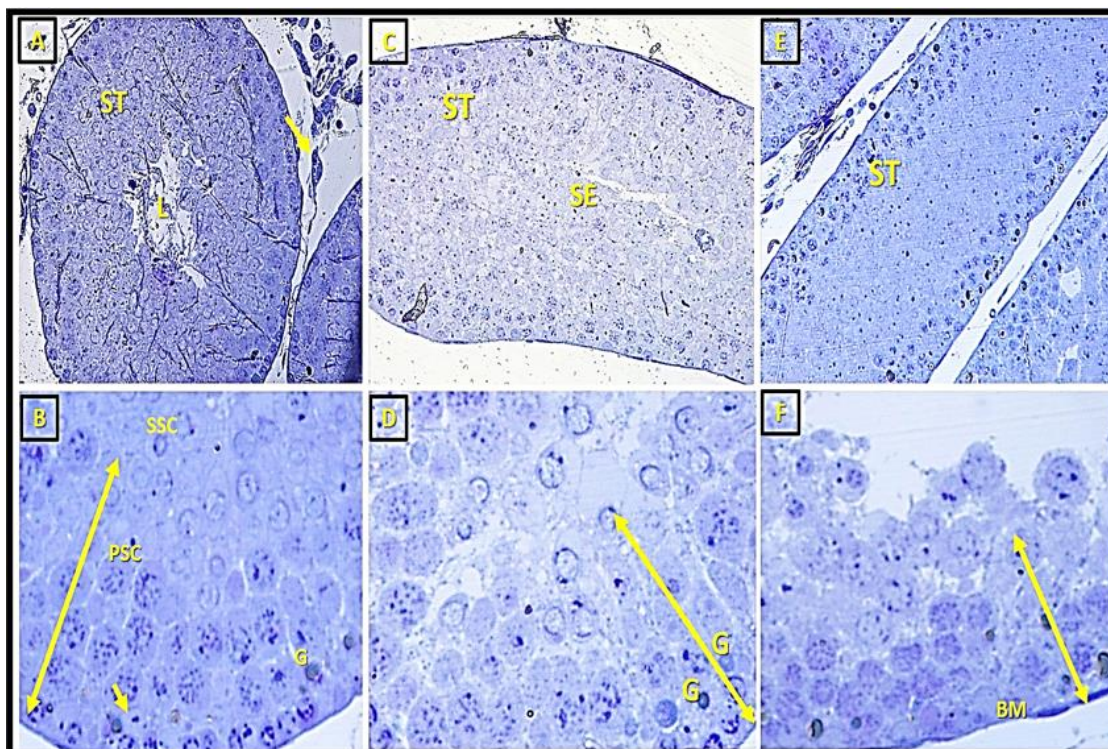


Fig.2A: A transverse section of albino rat testis from group I showing regular and well-defined outline of seminiferous tubules (ST) and narrow lumen(L). The tubules appear separated by thin interstitial tissue(I)contains leydig cell (yellow arrow) (x400). A higher magnification (**fig.2B**) showing full thickness of germinal epithelial lining of seminiferous tubules (yellow double head arrow); the Sertoli cell appears with pale staining and active mitotic figures (Yellow arrow). The primary spermatocyte (PSC) appears with large size and multiple nucleoli. Secondary spermatocyte appears small in size (SSC) with deeply stained nuclei(x1000). **Fig.2c:** showing distorted shape of seminiferous tubules (ST) with sloughed germ cells (SE) obliterating their lumen (x400). The higher magnification (**Fig.2D**): showing decreased thickness of germ cell layer lining the seminiferous tubules (yellow double head arrow) and decreased mitotic figures in the nuclei of mother Spermatogonia(G)(x1000). **Fig.2E:** showing distorted seminiferous tubules(ST) (x200). The higher magnification showing marked decrease in thickness of germ cell lining (double head arrow), decreased mitotic figures of different stages of germinal epithelial lining of the tubules and marked thinning of the basement membrane(BM). (Toluidine blue stain x1000).

Immunohistochemical Results:

The control group (I) exhibited a negative reaction to inducible nitric oxide synthetase (iNOS) in the germ cell layer of seminiferous tubules (Fig.3A). In contrast to the moderate reaction to iNOS observed in group II; the reaction appeared as brownish staining of the cytoplasm of the whole thickness of germ cell layer (Fig.3B). Sections of group III showed extensive reaction to iNOS, the reaction appeared as intense brownish staining of the cytoplasm of the whole thickness of germ cell layer lining the seminiferous tubules (Fig.3c).

Regarding the immunoreactivity to Ki67; group (I) revealed an intense positive reaction to

Ki67. The reaction appeared as intense brownish cytoplasmic staining of the whole thickness of the germ cell layer; but more concentrated in the cytoplasm and nuclei of the basal cell layer (Fig.4A). Moreover, group II sections revealed moderate reaction to ki67. The reaction was clearly observed in the superficial and intermediate germ cell layers but more intense in the basal cell layer (Fig.4B). Positive reaction to ki67 was observed also in sections obtained from group III; appeared concentrated only in the cytoplasm of basal cell layer (Fig 4C).

Concerning results of the TUNEL assay showed a negative reaction in sections of group I. No

apoptotic cells could be detected among the germ cell layer (Fig.5A). Moderate reaction was observed in sections obtained from group II; multiple apoptotic cells could be detected among

the germ cell layers (Fig.5B). Intense positive immune reaction was detected in all layers of the germinal epithelium of group III (Fig.5C).

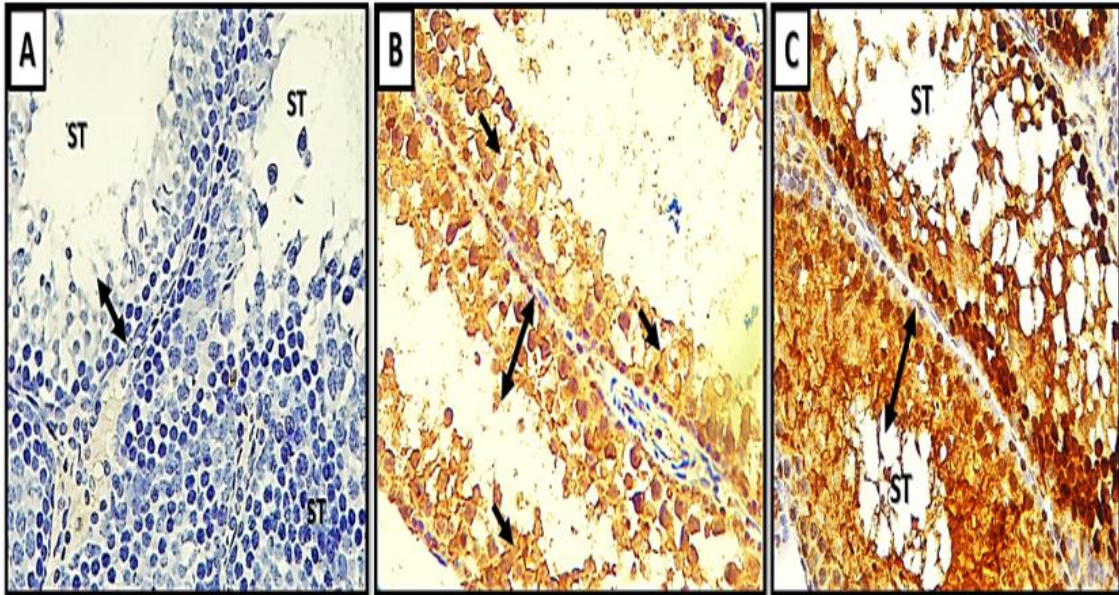


Fig.3A: A transverse section of albino rat testis from group (I) showing negative immune reaction to iNOS in the germ cell layer (double head arrow) of seminiferous tubules (ST). **Fig.3B:** showing moderate immune reaction to iNOS; the reaction appears as brownish staining of the cytoplasm (black arrows) of whole thickness of germ cell layer (double head arrow). **Fig.3C:** showing extensive immune reaction to iNOS, the reaction appears as intense brownish staining of the cytoplasm of whole thickness of germ cell layer lining the seminiferous tubules (ST) (double head arrow) (iNOSx400).

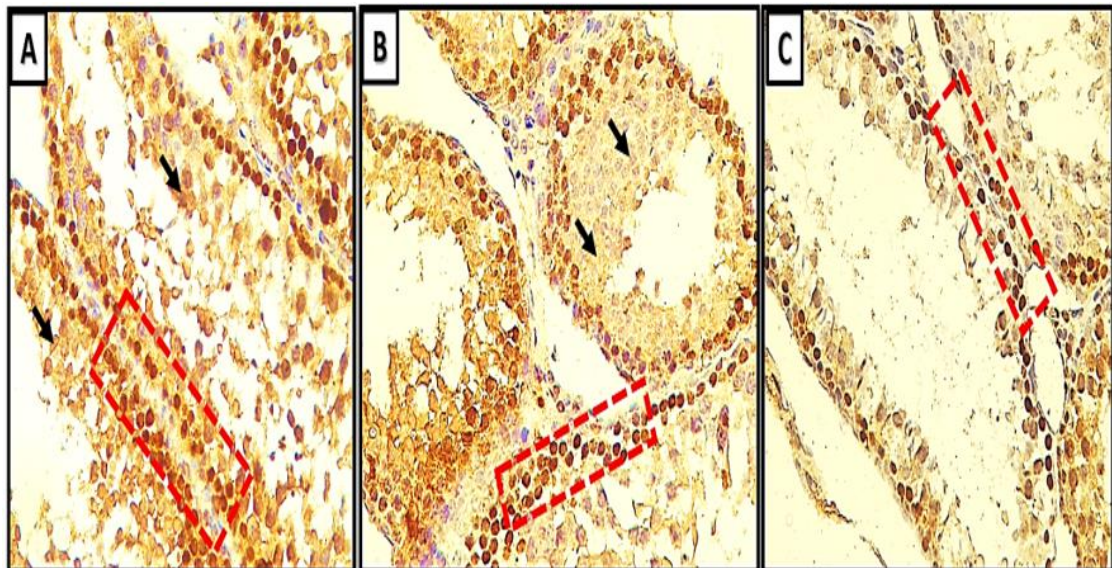


Fig.4A: A transverse section of albino rat testis from control group(I); showing intense reaction to Ki67 the reaction appears as moderate brownish cytoplasmic and nuclear staining (black arrows) of whole thickness of germ cell layer; note that the reaction is much more concentrated in the cytoplasm and nuclei of the basal cell layer (red inset). **Fig.4B:** showing moderate immune reaction to ki67 in the cytoplasm of superficial and intermediate germ cell layers(black arrows) but appears more intense in the basal cell layer (red inset). **Fig.4C:** showing intense immune reaction to ki67;the reaction appears concentrated only in the cytoplasm of basal cell layer note, the marked decrease of positively reacting cells(red inset)(Ki67x400).

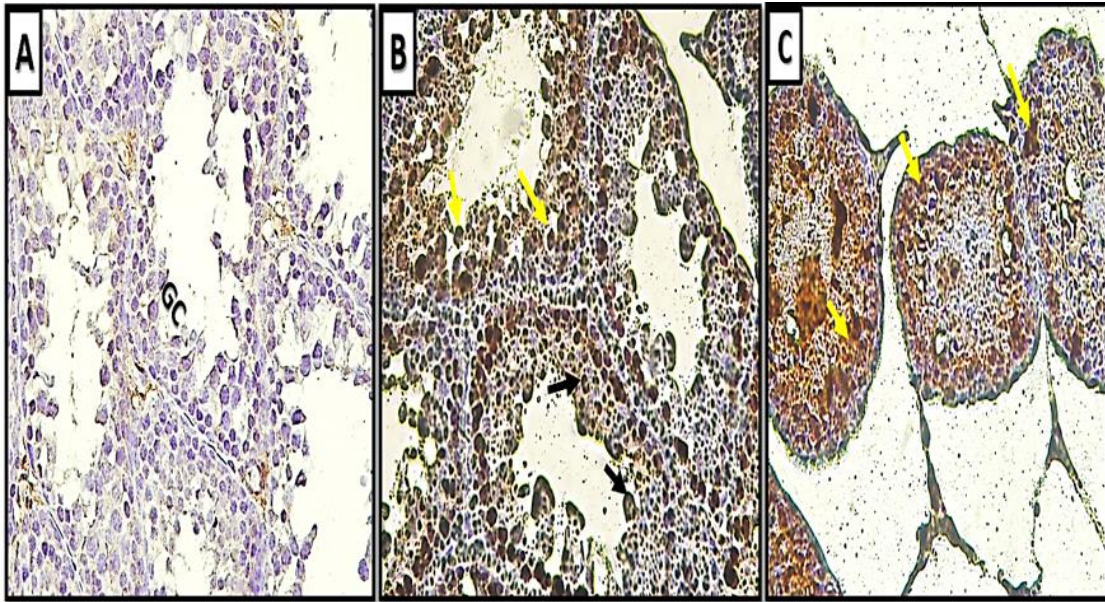


Fig.5A: A transverse section of albino rat testis from control group(I); showing negative immune reaction. No apoptotic cells could be detected among the germ cell layers. **Fig.5B:** showing moderate immune reaction; multiple apoptotic cells could be detected among the germ cell layer. It appears with dark staining of their cytoplasm and nuclei (yellow arrows). **Fig.5C:** showing intense immune reaction appears in all layers of germ cell lining of seminiferous tubules (yellow arrows). (TUNEL assayx400).

Results of Transmission Electron Microscopy:

Examination of transverse sections of albino rat testis from control group (I) by transmission electron microscopy revealed the germ cell lining of seminiferous tubules; Sertoli cells appeared resting on a basement membrane supported by myoid cells. Spermatogonia are arranged in one row and surrounded by dark cytoplasmic hallow. In addition, the primary spermatocyte exhibited a large size and well-defined circular nuclear membrane, apparent nucleolus and hypodense patchy chromatin (Fig.6A). The spermatogonia exhibited hypodense chromatin patches(fig.6B). The cytoplasm showed circular deeply stained ribosomes and mitochondria in their cytoplasm. With a higher magnification of the yellow inset area in Figure 6A; sertoli cell appeared with well-defined nuclear membrane and deeply stained nucleolus. The cytoplasm exhibited mitochondria with well-defined crista and thin filaments of the endoplasmic reticulum (Fig.6C).

Moreover, examining sections obtained from group (II) showed sertoli cells resting on the basement membrane supported by myoid cells. The spermatogonia appeared well organized, some spermatogonia appeared distorted with irregular nuclear membrane and clumped chromatin. The primary spermatocyte appeared with cytoplasmic vacuolations (Fig.7A). With higher magnification; Figure 7B showed sertoli cells with irregular nuclear membrane, and the cytoplasm exhibited some healthy mitochondria with well-defined crista; others appeared degenerated with distorted crista. In addition, the primary spermatocyte showed some degenerated mitochondria and distorted endoplasmic reticulum (Fig.7C).

On the other hand, severe degenerative signs were clearly observed in all types of cells of germinal epithelium in group III (fig.8A). Sertoli cells appeared with cytoplasmic vacuolations, dilated endoplasmic reticulum, rarified cytoplasm and degenerated mitochondria other cell

appeared shrunken with faint nuclear membrane (fig.8B). In addition, fig.8C showed other sertoli cell with irregular nuclear membrane, cytoplasmic vacuolations, degenerated mitochondria and smooth filaments of the endoplasmic reticulum. Secondary spermatocytes showed multiple cytoplasmic lipid droplets, marginal cytoplasmic vacuolations, dilated endoplasmic reticulum and disrupted Golgi complex (Fig.8D).

Furthermore, epididymal samples from control group (I) revealed a relatively high density of sperm distribution (9A) with apparent normal structure of the sperm tail; it appeared consisting of central axoneme, outer dense fibers, mitochondrial membrane and outer plasma membrane (inset). Moreover, group (II) showed moderate density of sperm distribution (Fig.9B). Section of group (III) exhibited very low density of sperm distribution (Fig.9C).

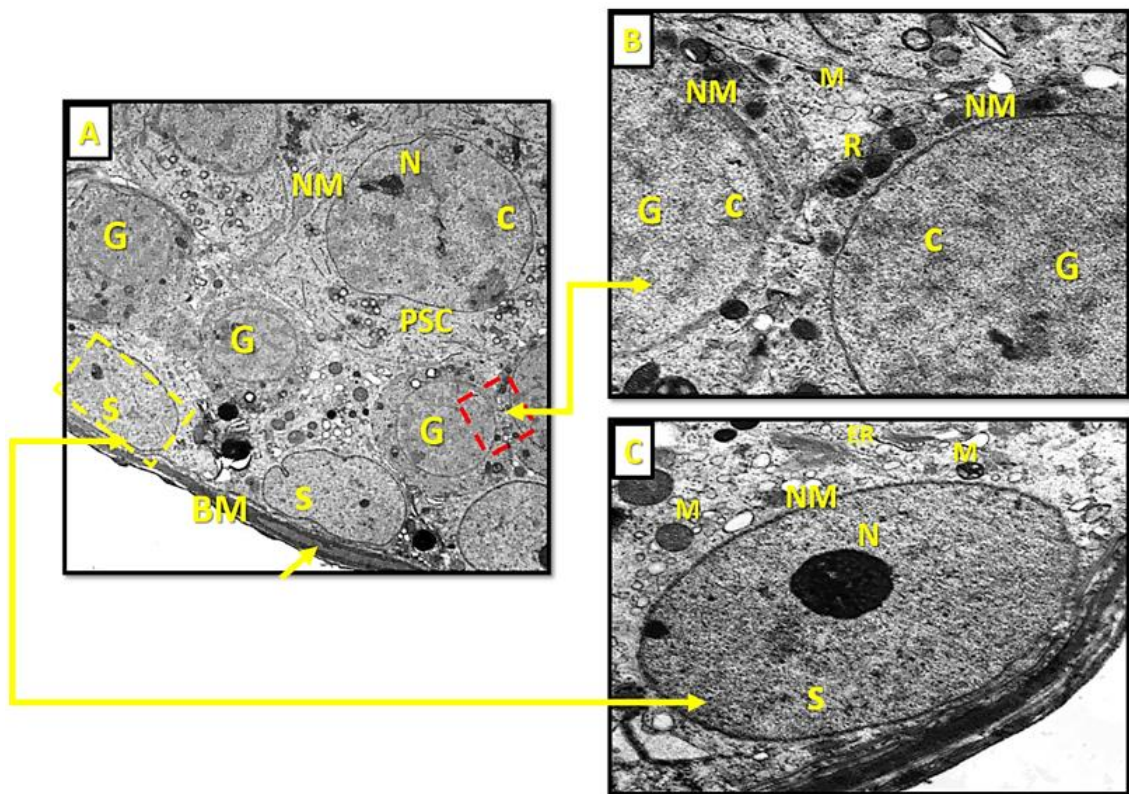


Fig.6A: A transverse section of albino rat testis from control group (I) showing the germ cell lining of seminiferous tubules; Sertoli cells (s) appears resting on basement membrane (BM) supported by myoid cells(yellow arrow).The Spermatogonia arranged in one row and surrounded by dark cytoplasmic hallow(G).The primary spermatocyte(PSC) are large in size with well-defined circular nuclear membrane(NM),apparent nucleolus(N) and hypodense patchy chromatin(C).With higher magnification to red inset area in **Fig.6A**. **Fig.6B** showing well defined circular nuclear membrane(NM) of the Spermatogonia(G) and hypodense chromatin patches (c). Circular deeply stained ribosomes(R) and mitochondria (M) are well detected in their cytoplasm. With higher magnification of the yellow inset; **Fig.6C** showing Sertoli cell(S) with well-defined nuclear membrane (NM) and deeply stained nucleolus(N). The cytoplasm showing the mitochondria with their crista(M) and thin filaments of the endoplasmic reticulum(SER). (Uranyl acetate/lead acetate x1000x4000, x3000).

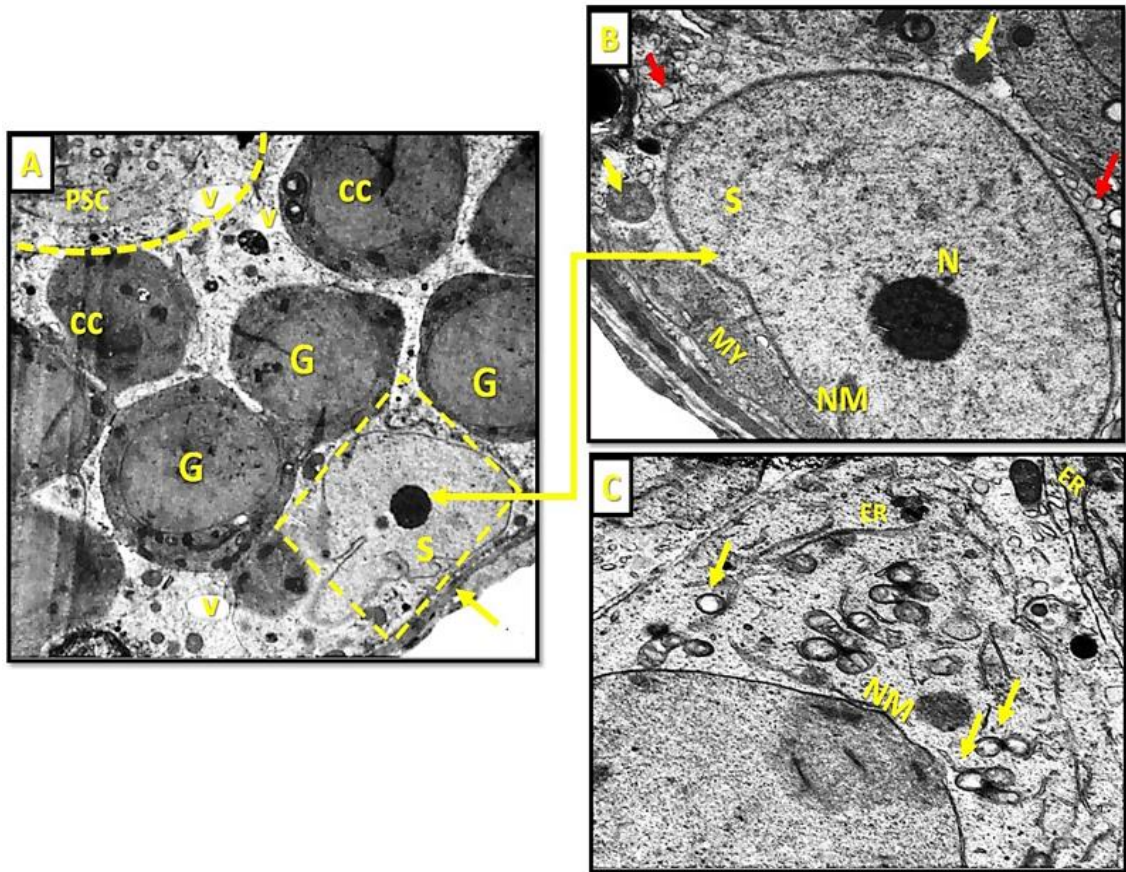


Fig.7A: A transverse section of albino rat testis from group (NMSII) showing Sertoli cell (S) resting on basement membrane (yellow arrow). The Spermatogonia appears arranged in one row(G),some Spermatogonia appear distorted with irregular nuclear membrane and clumped chromatin(C).The primary spermatocyte(PSC) appears with cytoplasmic vacuolations(v).With higher magnification to(yellow dotted inset); **Fig 7B** showing Sertoli cell (S) with irregular nuclear membrane (NM),deeply stained nucleolus (N); the cytoplasm showing some healthy mitochondria with well-defined crista(yellow arrows);others appear degenerated with distorted crista(red arrows). Sertoli cells appear resting on the basement membrane supported by myoid cells (MY). With higher magnification to the dotted encircled area; **Fig.7C** showing irregular nuclear membrane(NM) of (PSC), some degenerated mitochondria (yellow arrows) and distorted endoplasmic reticulum(ER). (Uranyl acetate/lead acetate x1500x3000 x4000).

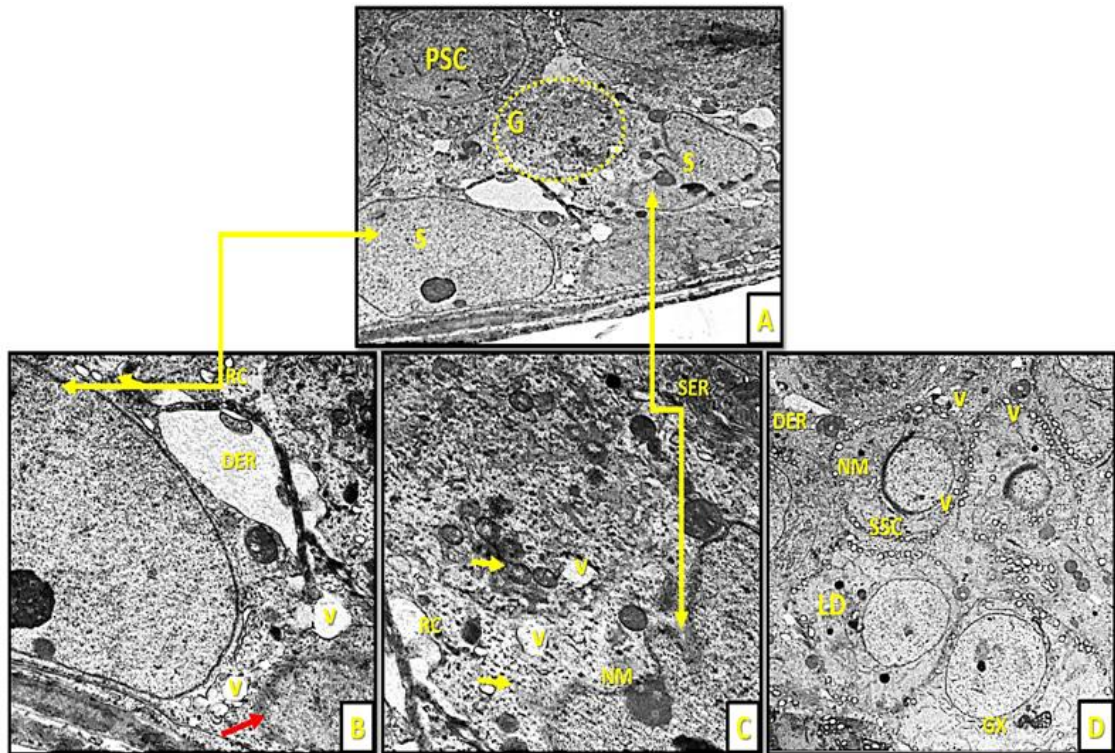


Fig.8A: A transverse section of albino rat testis from group (NMSIII) showing Sertoli cells (S), degenerated Spermatogonia (G) (encircled) and primary spermatocyte (PSC). With higher magnification in (**Fig.8B**); Sertoli cell appears with cytoplasmic vacuolations (V), dilated endoplasmic reticulum (DER), rarified cytoplasm (RC) and degenerated mitochondria (yellow arrow). Other Sertoli cell appears shrunken with faint nuclear membrane (red arrow). **Fig.8C:** showing other Sertoli cell with irregular nuclear membrane (NM), cytoplasmic vacuolations (v) and degenerated mitochondria (yellow arrow) and smooth filaments of the endoplasmic reticulum (SER). **Fig.8D:** showing the secondary spermatocytes (SSC) with thickened nuclear membrane (NM), cytoplasmic lipid droplets (LD), marginal cytoplasmic vacuolations (V), dilated endoplasmic reticulum (DER) and disrupted Golgi complex (GX). (Uranyl acetate/lead acetate x1500x3000x4000x1200).

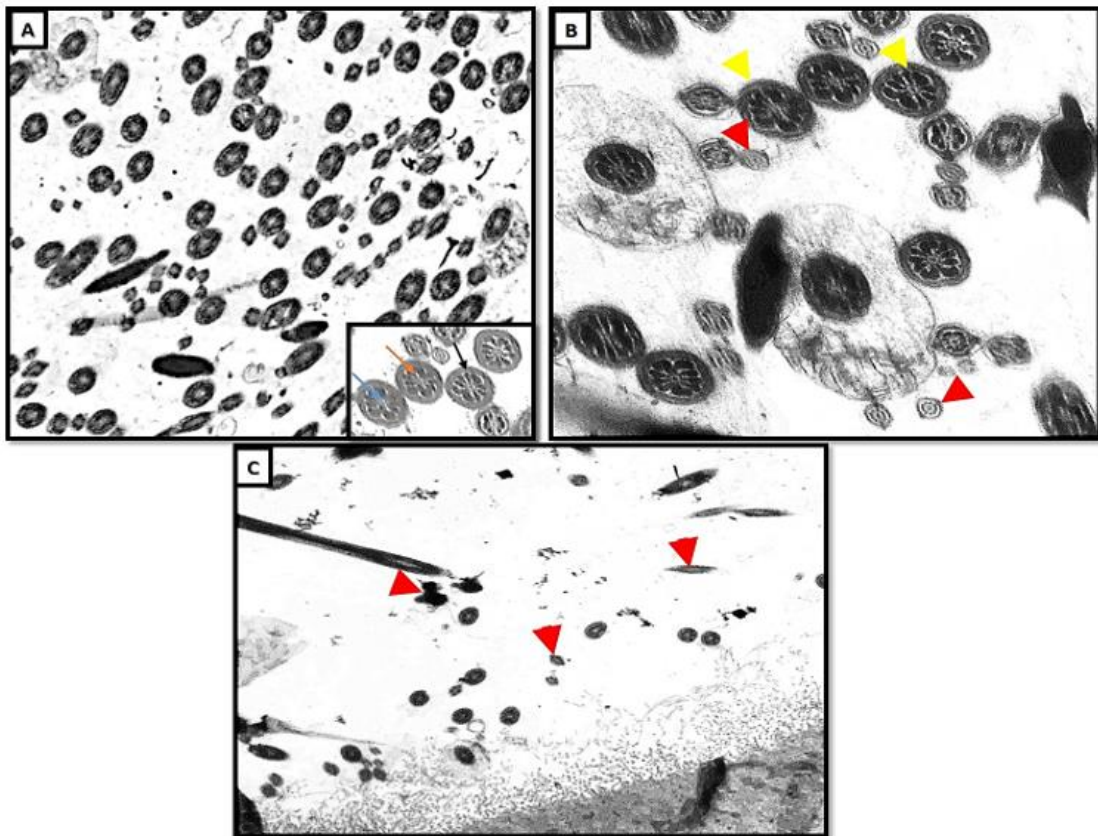


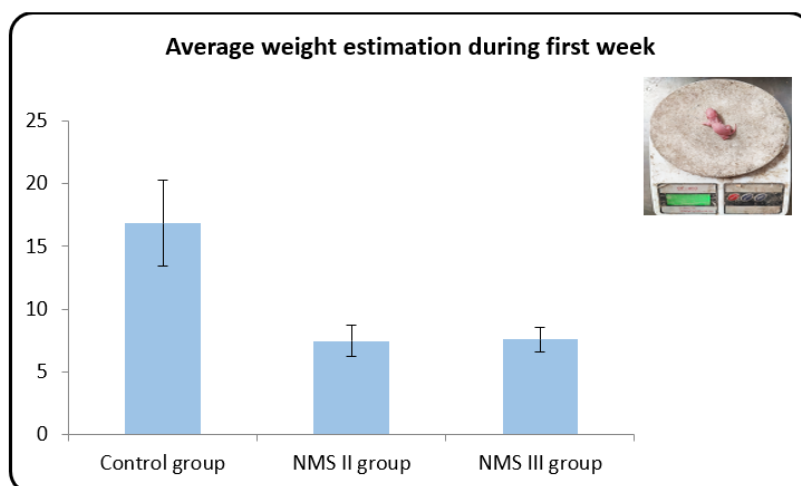
Fig.9A: A transverse section of epididymis from control group (I) showing normally appearing sperm tail structure with relative high density (x2500); the inset shows the sperm tail consisting of central axoneme (blue arrow head), outer dense fibers (red head arrow), and outer plasma membrane (black arrow head) (x5000). **Fig.(9B):** Electron micrograph of transverse section of epididymal sperm from (NMII) group showing relative low density of sperm number; some of sperm tails appear with normal structures (yellow arrow heads) and others appear disrupted (red arrow heads) (x3000). **Fig.(9C):** Electron micrograph of transverse section of epididymis from (NMIII) group showing extensive low density of sperm in epididymal tissue with apparently deformed appearance. (x3000) (Uranyl acetate/lead acetate)

Statistical Results:

Average Weight Gain Estimation During the First Week (Table 1/Histogram1):

In contrast to other groups, group III showed a statically significant decrease in average weight gain during the first week relative to group I P-value

< 0.05. On the other hand, there was no statistically significant decrease relative to group II P-value > 0.05 based on the data presented in (table 1). Group II demonstrated a highly significant decrease relative to group I, but no statistically significant decrease relative to group III P-value > 0.05.



Histogram (1): Contrast between control I, NMS II and NMS III groups regarding average weight estimation during 1st week.

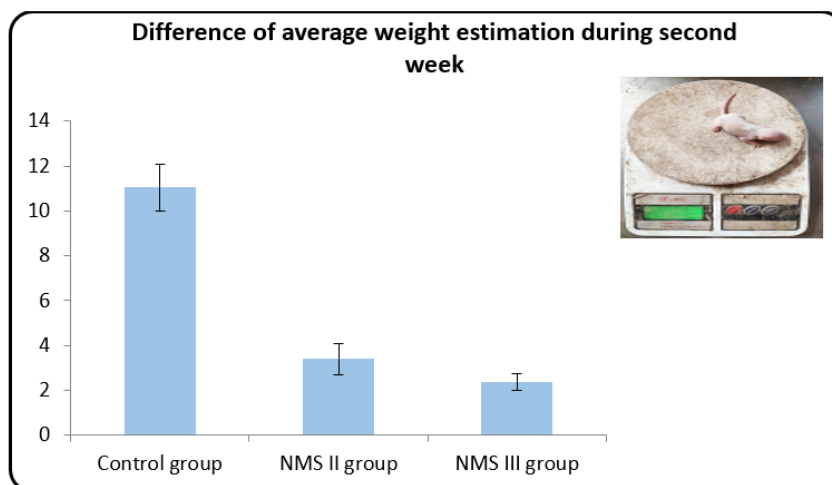
Average Weight Gain Estimation During the Second Week (Table 1/Histogram2):

Group III showed a statistically significant decrease in average weight gain during the second week relative to

groups I and II P-value < 0.05. On the other hand, group II showed a high statistically significant decrease relative to group I and a significant increase relative to group III P<0.05 (Table 1).

Table 1: Contrast between control I, NMS II and NMS III groups regarding average weight estimation during 1st and 2nd week and difference.

Average weight estimation		Control group No. = 7	NMS II group No. = 7	NMS III group No. = 7	Test value	P-value	Sig.
During 1 st week	Mean ± SD	5.82 ± 2.62	4.09 ± 0.98	5.22 ± 1.27	1.722•	0.207	NS
	Range	3 – 10	3 – 5.4	3.5 – 6.6			
During 2 nd week	Mean ± SD	16.86 ± 3.39	7.47 ± 1.24	7.59 ± 0.98	43.609•	<0.001	HS
	Range	12 – 22	6 – 10	6.3 – 8.9			
Difference	Mean ± SD	11.04 ± 1.05	3.39 ± 0.68	2.37 ± 0.35	279.588•	<0.001	HS
	Range	9 – 12	2.5 – 4.6	2 – 2.88			
Post Hoc analysis by LSD							
		Control Vs NMS II	Control Vs NMS III	NMS II Vs NMS III			
During 2 nd week		<0.001	<0.001	0.922			
Difference of average weight estimation		<0.001	<0.001	0.021			



Histogram (2): Contrast between control I, NMS II and NMS III groups regarding difference of average weight estimation during 2nd week

Statistical Results of MDA Levels In Rat Serum (Table2/Histogram3):

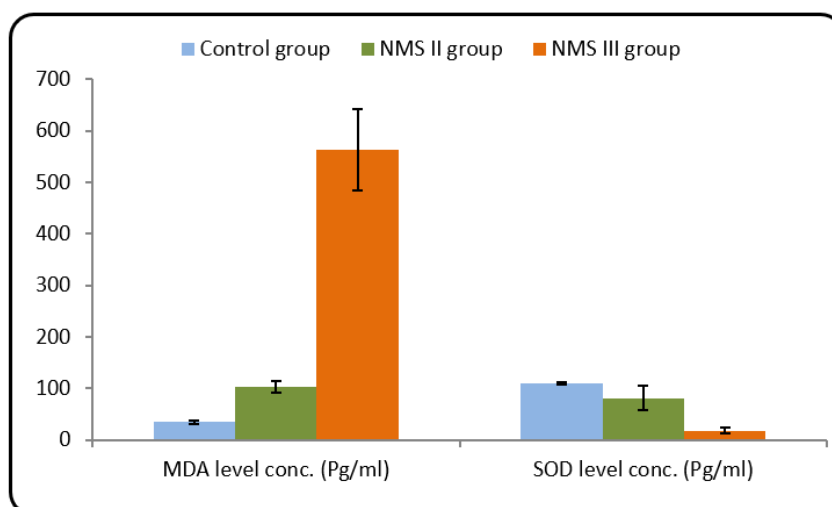
In contrast to other groups, group III showed a highly significant increase in the serum level of MDA relative to both groups I and II P-value < 0.05 based on the data presented in (table 2). Group II demonstrated a significant decrease relative to group III, but a significant increase relative to group I P-value < 0.05.

Statistical Results of SOD Levels In Rat Serum (Table2/Histogram3):

In contrast to other groups, group III showed a highly significant decrease in the serum level of SOD relative to both groups I and II P-value < 0.05 based on the data presented in (table2). Group II demonstrated a highly significant decrease relative to group I and a relative increase compared to group III P-value < 0.05.

Table 2: Contrast between control I, NMS II and NMS III groups regarding MDA and SOD levels

		Control group	NMS II group	NMS III group	Test value	P-value	Sig.
		No. = 7	No. = 7	No. = 7			
MDA level conc. (Pg/ml)	Mean ± SD	34.61 ± 3.74	103.86 ± 11.24	563.24 ± 79.97	265.210*	0.000	HS
	Range	30.62 – 39.4	91.86 – 118.35	487.33 – 700.44			
SOD level conc. (Pg/ml)	Mean ± SD	110.66 ± 2.14	81.31 ± 24.36	18.04 ± 6.14	74.046*	0.000	HS
	Range	104.55 – 120.33	43.43 – 103.85	14.45-20.77			
Post Hoc analysis by LSD							
		Control Vs NMS II	Control Vs NMS III	NMS II Vs NMS III			
MDA level conc. (Pg/ml)		0.012	0.000	0.000			
SOD level conc. (Pg/ml)		0.000	0.000	0.001			



Histogram (3): Contrast between control I, NMS II and NMS III groups regarding MDA and SOD levels.

Statistical Results of FSH/LH Hormone Levels in Rat Serum (Table 3/Histograms 4,5):

In contrast to other groups, group III showed no statistically significant increase in the serum level of FSH/LH hormones compared to both groups I and II P>0.05 based on the data presented in (table 3). Group II demonstrated no significant increase

relative to group I and no significant decrease compared to group III P>0.05

Statistical Results of Free Serum Testosterone Levels in Rat Serum (Table 3/Histogram 5):

In contrast to other groups, group III showed a statistically significant decrease in free serum testosterone level compared to both groups I and II P<0.05 based on the data presented in (table 3). Group II

demonstrated a statistically significant decrease relative to group I and a statistically significant increase compared to group III $P < 0.05$

Statistical Results of Serum ACTH/ Free Serum Cortisol Levels in Rat Serum (Table 3,4/Histograms 6,7):

In contrast to other groups, group III showed a significant increase in the serum ACTH and free serum cortisol level relative to both groups I and II $P < 0.05$ based on the data presented in tables (3,4). Group II demonstrated a significant decrease

relative to group III and a relative increase compared to group I $P < 0.05$.

Statistical Results of TSH/T3 Levels in Rat Serum (Tables 3,4/ Histograms 8,9):

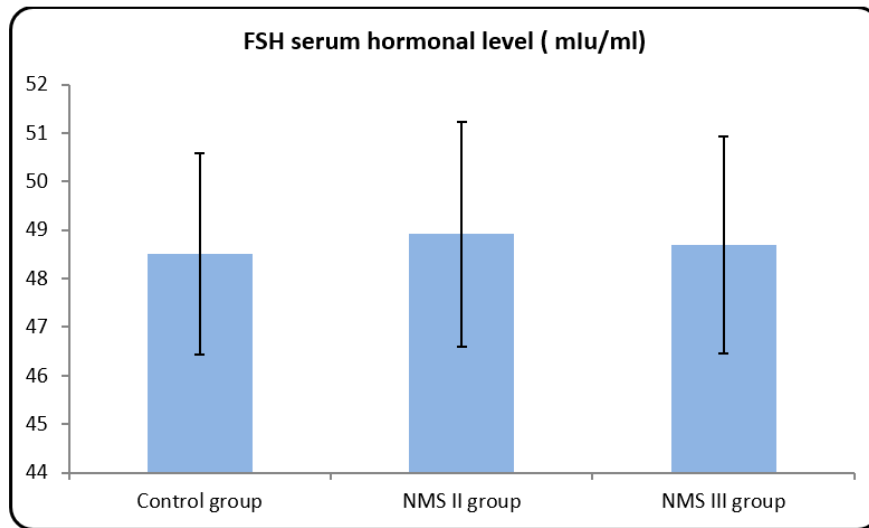
In contrast to other groups, group III showed a significant decrease in the serum level of TSH and free serum triiodothyronine levels relative to both groups I and II P -value < 0.05 based on the data presented in tables (3,4). Group II demonstrated a significant decrease relative to group I and a relative increase compared to group III $P < 0.05$.

Table 3: Contrast between control I, NMS II and NMS III groups regarding free serum testosterone, LH, FSH, TSH and serum cortisol levels.

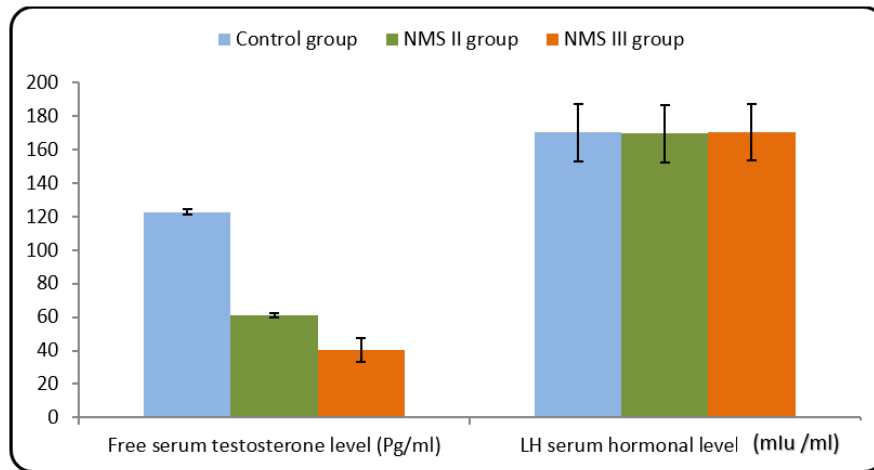
		Control group No. = 7	NMS II group No. = 7	NMS III group No. = 7	Test value	P-value	Sig.
Free serum testosterone level (ng/ml)	Mean \pm SD	122.59 \pm 1.62	61.01 \pm 1.24	40.52 \pm 7.15	691.909*	0.000	HS
	Range	120.44 – 124.66	58.82 – 62.33	30.23 – 50.44			
LH serum hormonal level (mIU/ml)	Mean \pm SD	170.25 \pm 17.12	169.58 \pm 17.01	170.68 \pm 16.86	0.007*	0.993	NS
	Range	140 – 190	140 – 190	141 – 191			
FSH serum hormonal level (mIU/ml)	Mean \pm SD	48.50 \pm 2.07	48.91 \pm 2.31	48.69 \pm 2.23	0.062*	0.940	NS
	Range	45.22 – 50.87	45.88 – 52.44	46.44 – 52.22			
TSH serum hormonal level (ng/ml)	Mean \pm SD	12.65 \pm 6.92	2.36 \pm 0.65	1.83 \pm 0.61	16.049*	0.000	HS
	Range	4.53 – 22.44	1.44 – 3.45	0.54 – 2.4			
Serum cortisol level (ng/ml)	Mean \pm SD	27.06 \pm 2.06	81.18 \pm 6.17	135.31 \pm 10.28	415.683*	0.000	HS
	Range	23.66 – 29.33	70.98 – 87.99	118.3 – 146.65			
Post Hoc analysis by LSD							
		Control Vs NMS II	Control Vs NMS III	NMS II Vs NMS III			
Free serum testosterone level (Pg/ml)		0.000	0.000	0.000			
TSH serum hormonal level (Pg/ml)		0.000	0.000	0.809			
Serum cortisol level (Pg/ml)		0.000	0.000	0.000			

Table 4: Comparison between control I, NMS II and NMS III groups regarding Tri-iodothyronine T3 serum level and ACTH serum level

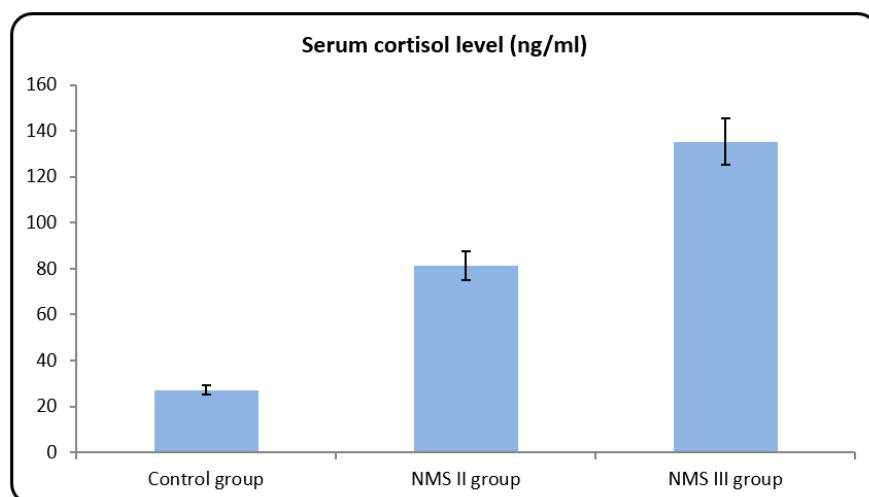
		Control group No. = 7	NMS II group No. = 7	NMS III group No. = 7	Test value	P-value	Sig.
Tri-iodothyronine T3 serum level (ng/ml)	Mean \pm SD	2.12 \pm 1.59	9.28 \pm 2.54	11.86 \pm 2.79	31.901*	<0.001	HS
	Range	0.72 – 5.06	5.22 – 12.88	8.44 – 16.2			
ACTH serum level (pg/ml)	Mean \pm SD	5.15 \pm 1.97	8.04 \pm 1.41	9.18 \pm 1.46	11.314*	0.001	HS
	Range	2.45 – 7.88	6.33 – 10.22	7.33 – 11.6			
Post Hoc analysis by LSD							
		Control Vs NMS II	Control Vs NMS III	NMS II Vs NMS III			
Tri-iodothyronine T3 serum level		<0.001	<0.001	0.056			
ACTH serum level		0.004	<0.001	0.207			



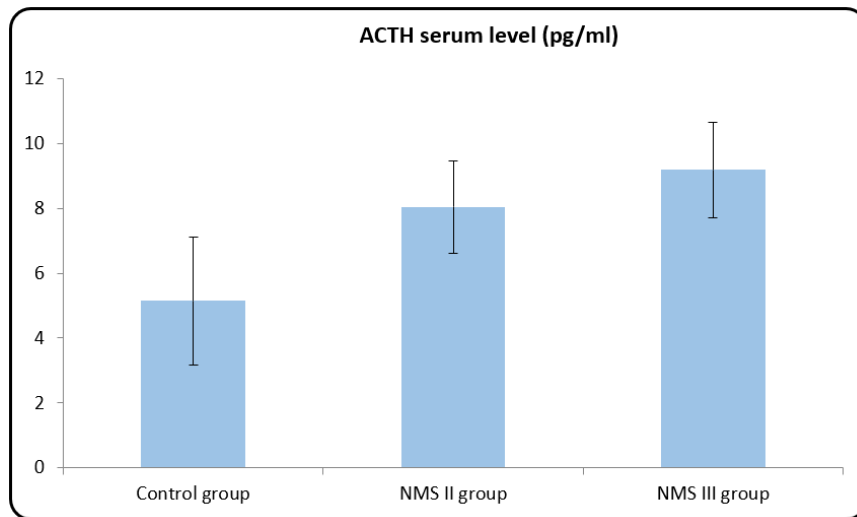
Histogram (4): Contrast between control I, NMS II and NMS III groups regarding FSH serum hormonal level



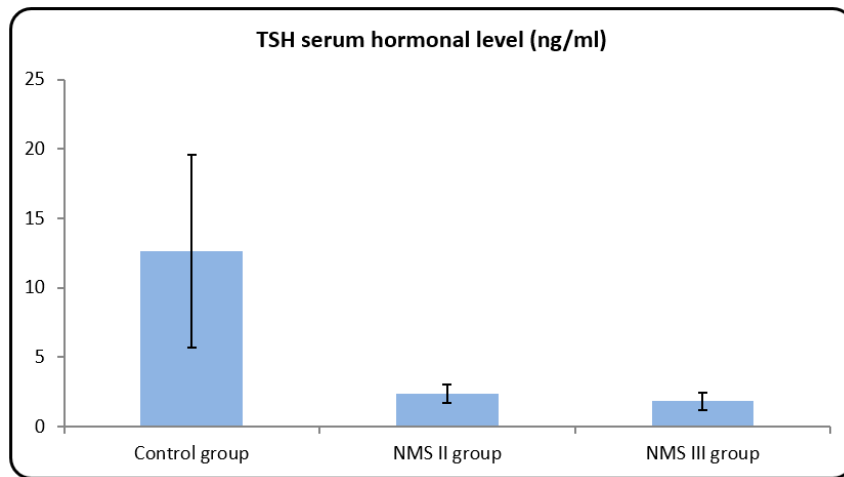
Histogram (5): Contrast between control I, NMS II and NMS III groups regarding free serum testosterone and LH levels.



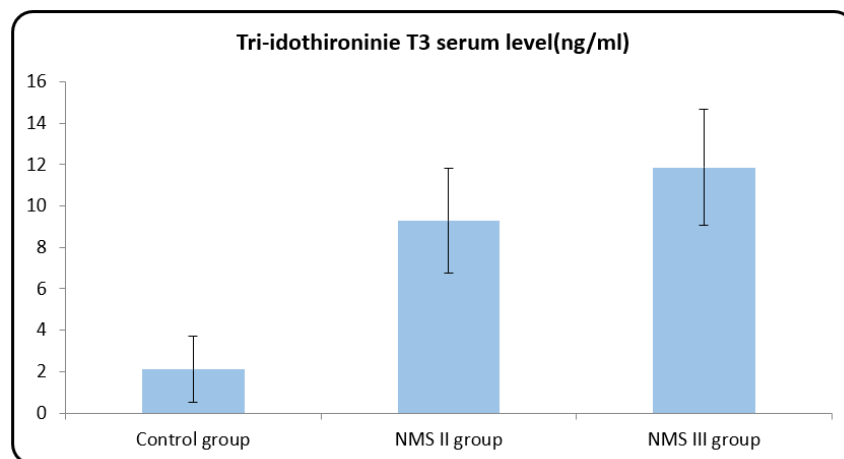
Histogram (6): Contrast between control I, NMS II and NMS III groups regarding serum cortisol level.



Histogram (7): Contrast between control I, NMS II and NMS III groups regarding ACTH serum level.



Histogram (8): Contrast between control I, NMS II and NMS III groups regarding TSH serum hormonal level.



Histogram (9): Contrast between control I, NMS II and NMS III groups regarding Tri-iodothyronine T3 serum level.

Morphometric Results:**Statistical Results of Seminiferous Tubules Diameter measurement (Table 5/Histogram 10):**

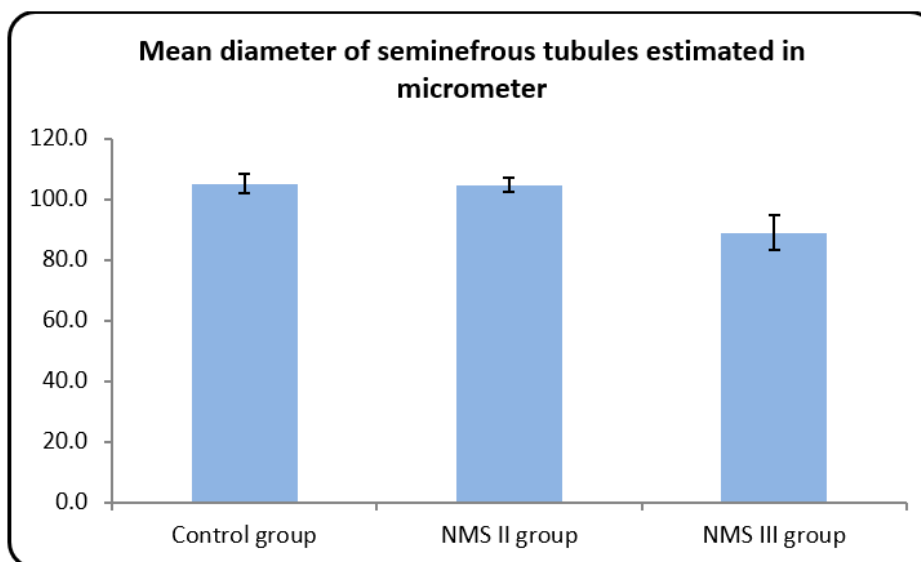
Concerning the diameter of seminiferous tubules, group III showed a significant decrease in seminiferous tubule diameter relative to both groups I and II $P < 0.05$ based on the data presented in (table 5). Group II demonstrated no statistically significant decrease in the tubule diameter relative to the group I $P > 0.05$. In addition, group III showed a statistically significant decrease compared to group II $P < 0.05$.

Statistical Results of Measurement of Germinal Epithelial Height of Seminiferous Tubules (Table 5/Histogram 11):

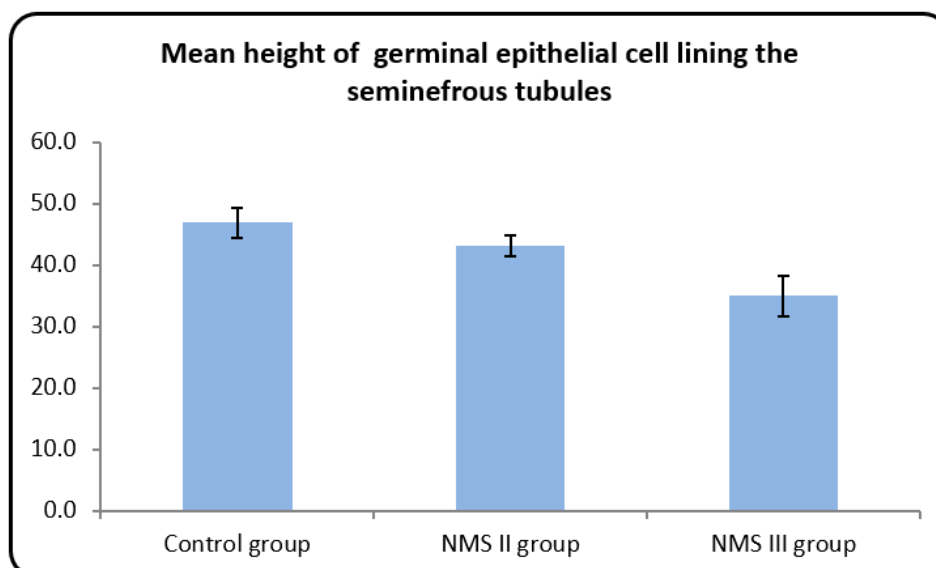
Regarding the height of germinal epithelium, group III showed a significant decrease in the thickness of the germ cell layer relative to both groups I and II $P < 0.05$ based on the data presented in (table 5). Group II demonstrated a significant decrease relative to group I and a relative increase compared to group III $P < 0.05$.

Table 5: Comparison between control I, NMS II and NMS III groups regarding mean diameter of seminiferous tubules estimated in micrometer and mean height of germ cell epithelial lining of the seminiferous tubules.

		Control group No. = 7	NMS II group No. = 7	NMS III group No. = 7	Test value	P-value	Sig.
Mean diameter of seminiferous tubules estimated in micrometer	Mean \pm SD	105.13 \pm 3.20	104.76 \pm 2.32	88.93 \pm 5.74	36.989*	0.000	HS
	Range	100.32 – 109.96	101.55 – 107.44	77.88 – 95.44			
Mean height of epithelial lining of germ cell lining the seminiferous tubules	Mean \pm SD	46.88 \pm 2.49	43.15 \pm 1.72	34.98 \pm 3.32	38.677*	0.000	HS
	Range	43.65 – 50.22	40.3 – 45.22	29.12 – 38.44			
Post Hoc analysis by LSD							
		Control Vs NMS II	Control Vs NMS III	NMS II Vs NMS III			
Mean diameter of seminiferous tubules estimated in micrometer		0.864	0.000	0.000			
Mean height of epithelial lining of germ cell lining the seminiferous tubules		0.015	0.000	0.000			



Histogram (10): Contrast between control I, NMS II and NMS III groups regarding mean diameter of seminiferous tubules estimated in micrometer.



Histogram (11): Contrast between control I, NMS II and NMS III groups regarding mean height of germinal epithelial cell lining the seminiferous tubules.

Statistical Results of Measurement of Area % of iNOS Immunoreactivity (Table 6/Histogram 12):

In contrast to other groups, group III showed a significant increase in % of immunoreactivity to iNOS relative to group I $P < 0.05$ and no statistically significant increase relative to group II based on the data presented in (table 6). Group II demonstrated no significant decrease relative to group III $P > 0.05$ and no significant increase compared to group I $P < 0.05$.

Statistical Results of Measurement of Area % of TUNEL Immunoreactivity (Table 6/Histogram 12):

In contrast to other groups, group III showed a significant increase in % of immunoreactive cells to TUNEL

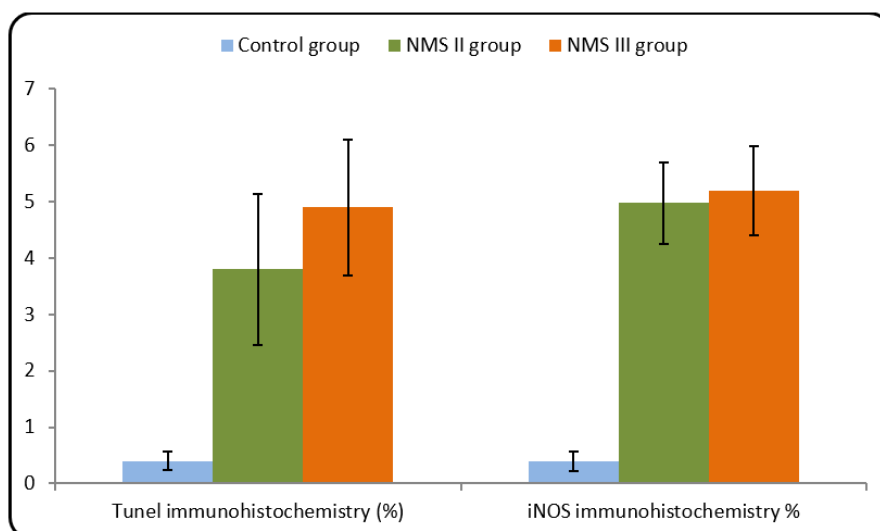
relative to both groups I and II $P < 0.05$ based on the data presented in (table 6). Group II demonstrated a significant increase relative to group I and a statistically significant decrease compared to group III $P < 0.05$.

Statistical Results of Measurement of Area % of Ki67 Immunoreactivity (Table 6/Histogram13):

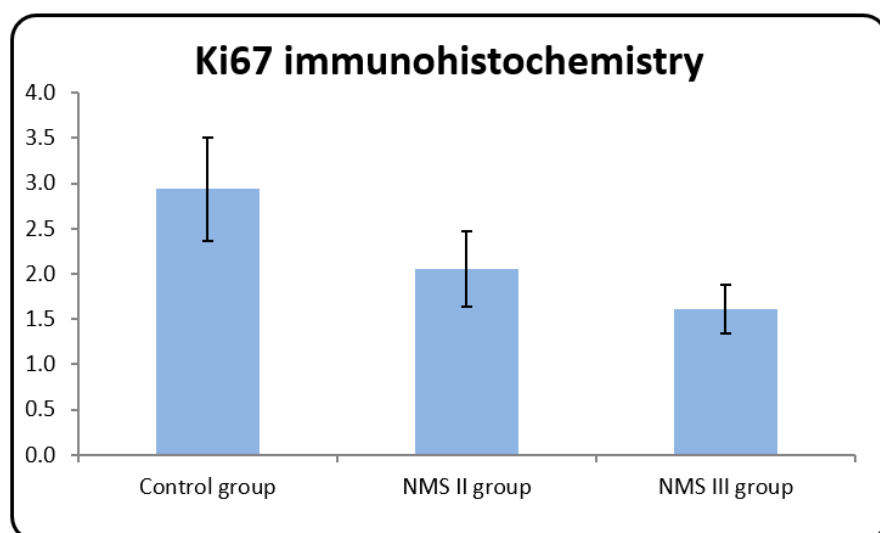
In contrast to other groups, group III showed a significant decrease in % of immunoreactivity to Ki67 relative to both groups I and II $P < 0.05$ based on the data presented in (table 6). Group II demonstrated a significant increase relative to group III and a relative decrease compared to group I $P < 0.05$.

Table 6: Contrast between control I, NMS II and NMS III groups regarding TUNEL immunohistochemistry, iNOS immunohistochemistry and Ki67 immunohistochemistry.

		Control group No. = 7	NMS II group No. = 7	NMS III group No. = 7	Test value	P-value	Sig.
TUNEL immunohistochemistry (%)	Mean ± SD	0.40 ± 0.16	3.80 ± 1.34	4.90 ± 1.21	35.163•	0.000	HS
	Range	0.18 – 0.66	1.94 – 5.65	2.95 – 6.01			
iNOS immunohistochemistry %	Mean ± SD	0.39 ± 0.17	4.98 ± 0.73	5.19 ± 0.79	130.522•	0.000	HS
	Range	0.16 – 0.68	3.92 – 5.77	3.95 – 6.01			
Ki67 immunohistochemistry %	Mean ± SD	2.94 ± 0.57	2.05 ± 0.41	1.61 ± 0.27	16.815•	0.000	HS
	Range	1.95 – 3.59	1.22 – 2.44	1.32 – 2.14			
Post Hoc analysis by LSD							
		Control Vs NMS II	Control Vs NMS III	NMS II Vs NMS III			
TUNEL immunohistochemistry (%)		0.000	0.000	0.064			
iNOS immunohistochemistry %		0.000	0.000	0.534			
Ki 67immunohistochemistry %		0.001	0.000	0.076			



Histogram (12): Contrast between control I, NMS II and NMS III groups regarding TUNEL immunohistochemistry and iNOS immunohistochemistry.



Histogram (13): Contrast between control I, NMS II and NMS III groups regarding Ki67 immunohistochemistry

DISCUSSION

Early postnatal exposure to stressors can affect brain development and the formation of biological networks. Stress stimulates the adrenergic system and modifies the endocrine and immune systems' functions (Kostenko *et al.*, 2019). According to previous studies, stress is a significant factor in disrupting fertility (Kilic *et al.*, 2021) (Pałkowska-Goździk *et al.*, 2017). Intimate maternal-child bonding is vital for the growth and development of biological systems. Moreover, the level of numerous hormones in neonates is altered when they are deprived of critical stimuli during separation from their mothers, including

emotional distress, loss of skin-to-skin contact with the mother, loss of body temperature, malnutrition, and other unidentified factors (Wang *et al.*, 2023). It has been further demonstrated that the hypothalamic-pituitary-thyroid (HPT), hypothalamic-pituitary-gonadal (HPG) and hypothalamic-pituitary-adrenal (HPA) axes have important roles in the regulation of many homeostatic systems including the metabolic system, reproductive system and immune system. Despite this, the intimate relation between NMS and the disturbance in those axes is still a matter of recent research work (Gehrand *et al.*, 2020).

The current study examined the histological, ultrastructural, immunohistochemical and biochemical effects of early NMS on the testis of male albino rats. Thirty pregnant dams were utilized in the current work and subdivided into groups (i), (ii) and (iii). After parturition, neonates were also randomly divided into three groups: control group (I), neonatal maternal separation group (NMS II) in which the pups were separated from their dams for 2 hours per day, and neonatal maternal separation group (NMSIII) in which the pups were separated from their dams for 4 hours per day from PND0 to PND14. The objective of this study was to establish the correlation between histological and immunohistochemical alterations observed in the testis of rats following neonatal maternal separation with the attenuation of hypothalamic-pituitary-thyroid-adrenal and gonadal axes.

Histological and morphometric results of the present study revealed different degrees of affection of testicular parenchyma in both groups (NMSII) and (NMSIII); examination of sections from both groups revealed disrupted seminiferous tubules with a marked decrease in their diameter and widened interstitium. In addition to decreased thickness of the germ cell layer in group III relative to group II and between both groups relative to the control group I. Furthermore, immunohistochemical results revealed that the number of proliferating (Ki67-positive) cells was substantially reduced in both the 2-h/day and 4-h/day NMS groups relative to the control group. Moreover, the number of apoptotic cells was significantly altered between groups II and III. Previous results could be attributed to the fact that NMS substantially increased the production of reactive oxygen species, causing extensive damage to nucleic acids, proteins, lipids, and activating apoptosis. In addition, the marked imbalance between the rate of proliferating cells, as indicated by the Ki67 assay, and the rate of apoptotic cells,

as exhibited by the TUNEL assay, could explain the difference between groups in the height of the germinal epithelial lining and active mitotic figures detected in seminiferous tubules in semithin sections.

Liu *et al.*, (2022) & Somade *et al.*, (2023) mentioned that the ability of testicular tissue to synthesize NO can be reflected by measuring total NOS and iNOS activities. The current study revealed a marked increase in iNOS immunoreactivity in neonatal separation groups II and III. Statistical results also revealed a marked increase in the area percentage of iNOS immune stained areas in group III relative to both groups I and II.

On the other hand, malondialdehyde (MDA) is the byproduct of lipid peroxide production and its concentration can indirectly reflect the level of free radicals and the degree of lipid peroxidation, as well as the extent of testicular germ cell injury (Pałkowska-Goździk *et al.*, 2017) (Jing *et al.*, 2023). Conversely, superoxide dismutase (SOD) is an indispensable antioxidant enzyme that protects against oxidative damage and is one of the most important substances for removing reactive oxygen species. The level of SOD can indicate the antioxidant capacity of all tissues (Mokhtar *et al.*, 2021).

Enzymes linked to oxidative stress were impacted by the psychological strain induced by maternal separation (Awadalla *et al.*, 2023). According to the findings of the present study; NMS II and III demonstrated a notable reduction in SOD and a substantial elevation in serum MDA.

Gonsioroski *et al.*, (2020) and Ibrahim *et al.*, (2019) clarified the normal signs of active cell function which could be detected by transmission electron microscopy (TEM) and were greatly correlated with the results of the present work; the cytoplasm of Sertoli cells in group I showed ring mitochondria and smooth filaments of endoplasmic reticulum. On the other hand, the primary spermatocyte appeared large in size with a well-defined circular nuclear

membrane, apparent nucleolus and hypodense patchy chromatin. The cytoplasm showed circular deeply stained ribosomes and mitochondria.

In contrast to the results of TEM obtained from group (NMSII); the Sertoli cell showed an irregular nuclear membrane, and a large number of degenerated mitochondria with distorted crista were detected in their cytoplasm. The spermatogonia appeared distorted with irregular nuclear membrane and clumped chromatin. The primary spermatocyte showed some degenerated mitochondria, distorted endoplasmic reticulum, irregular nuclear membrane and evident cytoplasmic vacuolations. Furthermore, Sertoli cells in group III appeared with cytoplasmic vacuolations, dilated endoplasmic reticulum, rarified cytoplasm and degenerated mitochondria. In addition, some degenerated spermatogonia and primary spermatocytes were also detected. The secondary spermatocytes appeared with a thickened nuclear membrane, multiple cytoplasmic lipid droplets, marginal cytoplasmic vacuolations, dilated endoplasmic reticulum and disrupted Golgi complex. All previous degenerative signs were much more evident in group (NMSIII) relative to both groups I and II.

In their study, Wang *et al.* (2023) elucidated the significant function of mitochondria in spermatogenesis, energy provision and autophagy-related protein regulation. The authors added that disruption of mitochondrial dynamics could potentially explain the mechanism underlying testicular injury, autophagy and apoptosis. Additionally, the mitochondrial dysfunction could impair the activation of Sirt1/Nrf2 pathway, which counteracts the detrimental effects of reactive oxygen species (ROS). This is greatly correlated with the findings of the current work which exhibited a considerable quantity of degenerated mitochondria in the cytoplasm of different cells of germinal epithelium in groups II and III.

On the other hand, morphometric and statistical results of the

current work revealed that there was a significant decrease in the height of germinal epithelium in the sections obtained from groups II and III. In addition to the decreased mitotic figures exhibited in both groups. Previous findings are explained by Hetz C& Papa FR. (2018) & Liu *et al.*, (2022) who attributed the previous findings to the endoplasmic reticulum stress (ERS). A dysfunctional endoplasmic reticulum compromises the protein folding mechanisms, leading to the accumulation of misfolded proteins. ERS is significantly involved in apoptosis and defects in cell differentiation. Authors added that the elevated levels of reactive oxygen species (ROS), impaired function of mitochondria and stress in the endoplasmic reticulum could potentially account for the inhibition of germ cell proliferation and reduction in mitotic figures observed in the germ cell lining of seminiferous tubules.

Demyashkin *et al.* (2023) explained the molecular basis for the disparity between the rates of proliferation and apoptosis and clarified its relation with the thickness of the germ cell layer. The author added that, the activation of protein kinase B and phosphoinositide-3-kinase caused by the presence of reactive oxygen species (ROS), enhances the permeability of the germ cell layer and disrupts homeostasis. This is accompanied by injury to lipids that are heavily deposited in the vesicles of Leydig cells and serve as a source of cholesterol for sex hormone synthesis; consequently, testosterone synthesis is reduced.

Regarding the level of different hormones of the hypothalamic-pituitary axis, there was no statistically significant difference in the serum levels of LH and FSH hormones between groups II and III and the control group, as determined by the results of the present study. In contrast, both TSH and T3 hormone levels decreased significantly in the serum samples of both groups II and III. Previous results are in accordance with Gehrand *et al.*, (2016) and Son *et al.*,

(2022) who explained the previous results by the deprivation of various critical stimuli during the separation of neonates from their mothers, including emotional distress, loss of skin-to-skin interaction with the mother, loss of body temperature, malnutrition, and other unknown factors. It is believed that these effects alter the hormone levels of newborns.

Special concern is given to the thyroid hormone level in neonates because it has an essential role in the maturation of the male reproductive system. The current study revealed that there were decreased serum levels of TSH and free T₃; which may be explained by malnutrition resulting from the maternal separation. Wen *et al.*, (2022) performed a prenatal diet restriction of pregnant rats from day 11 to day 21 and proved that prenatal food restriction could induce dysfunction of the hypothalamic-pituitary-adrenal (HPA) axis in the adult offspring. In addition, decreased serum levels of TSH and free T₃; may be also explained by the disturbance in weight gain and malnutrition that occurred in early neonatal life resulting from the maternal separation. The author added that the longer the period of maternal separation; the more that the pups became malnourished and more affection for thyroid hormonal profiles could be exhibited.

In contrast with the results of the present work, Cooke *et al.* (1991) & Cooke&Meisami (1991) proved that neonatal treatment with propylthiouracil; an inhibitor of thyroid hormone synthesis, has been shown to cause an increase in testicular weight and sperm number.

Jaimes-Hoy *et al.* (2016), Palkowska-Goździk *et al.* (2017) and O'Kane *et al.* (2018) demonstrated that malnutrition or starvation associated with NMS resulted in the expected down-regulation of HPT axis activity in rodents, although the magnitude of the response is variable according to sex. In addition, the study demonstrated that NMS in males may be associated with a slight secondary hypothyroidism; decreased TSH and T₃

serum concentrations in adulthood with increased Trhde mRNA expression levels; this would be associated with an increase in the inactivation of released thyroid release hormone (TRH) prior to its entry into the portal vessels, resulting in decreased TSH secretion.

Moreover, group II exhibited a statistically significant increase in serum cortisol levels compared to the control group, while group III demonstrated an increase in cortisol levels relative to both groups I and II. Previous results may be comprehensible by the fact that stress in early life induces neuroendocrine system changes. In this regard, prior research had demonstrated that both moderate and severe stressors could induce the secretion of corticosterone and ACTH in individuals with MS.

Gonadal function is significantly regulated by glucocorticoids at various levels of the hypothalamus-pituitary-adrenal (HPA) axis, including the gonads, pituitary gland, and hypothalamus. Hence, disturbance in the secretion of glucocorticoids may impede the physiological processes of the reproductive system Widström *et al.*, (2019).

Kageyama *et al.* (2021) asserted that modifications in these hormones have the potential to impact the sympathetic and parasympathetic nervous systems, thereby inducing a direct disturbance in testicular function. The author added that, maternal separation-induced stress during postnatal days 2 to 15 may impede the formation of the hypothalamic-pituitary-thyroid and gonadal axes, leading to increased corticosterone levels and subsequent immunological and behavioral modifications during adulthood.

Conclusion:

However, the consequences of NMS on various organs are well-documented, the precise effects of NMS on the male reproductive system remain obscure. An experimental model was established in this study to assess the adverse effects of NMS on the structure, ultrastructure and function of the male

albino rat testis. Emotional distress, loss of skin-to-skin contact, hypothermia and malnutrition induced by NMS impaired the development, structure, ultrastructure and function of the male reproductive system. The experimental model utilized in this study simulates the growing incidence of premature or low-birth-weight infants that have been confined to neonatal intensive care units (NICUs) within medical facilities. Additionally, significant attenuation of different hormones of hypothalamic-pituitary-thyroid-adrenal and gonadal axes has been proved as a result of neonatal maternal separation; this led to conspicuous histological, immunohistochemical, and ultrastructural alterations. Further investigations are necessary to ascertain the exact impacts of NMS on the male reproductive system in both animals and humans.

Declarations:

Ethical Approval: With approval number FWA 000017585, the Ethical Committee of Ain Shams University granted approval for the study. The methods used in the current study were implemented in adherence to the guidelines of (CARE). The committee of research ethics of Ain Shams University, the local medical school.

Funding: No funding was received.

Availability of Data and Materials: All datasets analysed and described during the present study are available from the corresponding author upon reasonable request.

Acknowledgements: We acknowledge all participants in this work.

REFERENCES

- Awadalla, E.A., Abd El, A.E.K.M., Kader, S.A., *et al.*, (2023): Oxidative and inflammatory disruptions of hypothalamic-pituitary-testicular axis by Octylphenol and protective role of alpha lipoic acid: histological and biochemical studies. *Journal of Biological Regulators and Homeostatic Agents*, Vol. 37 » Issue (5): 24452455. DOI: 10.23812/j.bio
- l.regul.homeost.agents.2023370 5.241
- Bancroft, J.D & Gamble, M. (2008): Theory and practice of histological techniques. Elsevier health sciences. 6th Edition, Churchill Livingstone, Elsevier, China.
- Bodensteiner KJ, Christianson N, Siltumens A, *et al.*, (2014): Effects of early maternal separation on subsequent reproductive and behavioral outcomes in male rats. *Journal of General Psychology*, 2014;141(3):228-46. doi: 10.1080/00221309.2014.897215. PMID: 24940813.
- Cooke PS, Hess RA, Porcelli J, *et al.*, (1991): Increased sperm production in adult rats after transient neonatal hypothyroidism. *Endocrinology journal*, 1991 Jul;129(1):244-8. doi: 10.1210/endo-129-1-244. PMID: 2055187.
- Cooke PS & Meisami E. (1991): Early hypothyroidism in rats causes increased adult testis and reproductive organ size but does not change testosterone levels. *Endocrinology journal*, 129 (1):237-43. doi: 10.1210/endo-129-1-237. PMID: 2055186.
- Crombie GK, Palliser HK, Shaw JC, *et al.*, (2021): Effects of prenatal stress on behavioral and neurodevelopmental outcomes are altered by maternal separation in the neonatal period. *Psycho neuroendocrinology journal*, 124:105060. doi: 10.1016/j.psyneuen.2020.105060. Epub 2020 Nov 26. PMID: 33333379.
- Császár-Nagy N, Bókkon I., (2018): Mother-newborn separation at birth in hospitals: A possible risk for neurodevelopmental disorders? *Neuroscience Biobehavioral Reviews*, 84:337-351. doi: 10.1016/j.neubiorev.

- 2017.08.013. Epub 2017 Aug 26. PMID: 28851575.
- Demyashkin GA, Vadyukhin MA, Shekin VI. (2023): The Influence of Platelet-Derived Growth Factors on the Proliferation of Germinal Epithelium After Local Irradiation with Electrons. *Journal of Reproductive Infertility*, 24(2):94-100. doi: 10.18502/jri.v24i2.12494. PMID: 37547573; PMCID: PMC10402459.
- Duan WR, Garner DS, Williams SD, Funckes-Shippy CL, Spath IS, Blomme EA. (2003): Comparison of immunohistochemistry for activated caspase-3 and cleaved cytokeratin 18 with the TUNEL method for quantification of apoptosis in histological sections of PC-3 subcutaneous xenografts. *Journal of Pathology*, 199(2):221-8. doi: 10.1002/path.1289. PMID: 12533835.
- Eskandari F, Salimi M, Binayi F, *et al.*, (2023): Investigating the effects of maternal separation on hypothalamic-pituitary-adrenal axis and glucose homeostasis under chronic social defeat stress in young adult male rat offspring. *Neuroendocrinology journal*, 113(3):361-380. doi: 10.1159/000526989. Epub 2022 Sep 9. PMID: 36088912.
- Gehrand AL, Phillips J, Malott K, *et al.*, (2020): Corticosterone, adrenal, and the pituitary-gonadal axis in neonatal rats: effect of maternal separation and hypoxia. *Endocrinology journal*, 161(7): bqaa085. doi: 10.1210/endo/bqaa085. PMID: 32459830; PMCID: PMC7310600.
- Gonsioroski A, Mourikes VE. and Flaws JA (2020): Endocrine Disruptors in Water and Their Effects on the Reproductive System. *International Journal of Molecular Sciences*, 21(6):1929. doi: 10.3390/ijms21061929. PMID: 32178293; PMCID: PMC7139484.
- Hetz C and Papa FR. (2018): The Unfolded Protein Response and Cell Fate Control. *Molecular Cell journal*, 18;69(2):169-181. doi: 10.1016/j.molcel.2017.06.017. Epub 2017 Nov 5. PMID: 29107536.
- Hodes, G.E. and Kropp, D.R., (2023): Sex as a biological variable in stress and mood disorder research. *Nature Mental Health*, 1(7), pp.453-461.
- Ibrahim, A.I., Amira, F.A., Manal, M.M. *et al.*, (2019): Effect of zinc oxide nanoparticles on the structure of testis of adult albino rats and the possible protective role of naringin. *The Medical Journal of Cairo University*, 87(September), pp.3469-3483.
- Jaimes-Hoy L, Gutiérrez-Mariscal M, Vargas Y, *et al.*, (2016): Neonatal Maternal Separation Alters, in a Sex-Specific Manner, the Expression of TRH, of TRH-Degrading Ectoenzyme in the Rat Hypothalamus, and the Response of the Thyroid Axis to Starvation. *Endocrinology journal*, 157(8):3253-65. doi: 10.1210/en.2016-1239. Epub 2016 Jun 20. PMID: 27323240.
- Jing J, Peng Y, Fan W, *et al.*, (2023): Obesity-induced oxidative stress and mitochondrial dysfunction negatively affect sperm quality. *FEBS Open Bio. Open access journal*, 13(4):763-778. doi: 10.1002/2211-5463.13589. Epub 2023 Mar 14. PMID: 36866962; PMCID: PMC10068321.
- Juruena MF, Bourne M, Young AH, *et al.*, (2021): Hypothalamic-Pituitary-Adrenal axis dysfunction by early life stress. *Neuroscience Letters journal*,

- 10; 759:136037. doi: 10.1016/j.neulet.2021.136037. Epub 2021 Jun 8. PMID: 34116195.
- Kageyama K, Iwasaki Y, and Daimon M. (2021): Hypothalamic Regulation of Corticotropin-Releasing Factor under Stress and Stress Resilience. *International Journal of Molecular Sciences*, 22(22): 12242. doi: 10.3390/ijms222212242. PMID: 34830130; PMCID: PMC8621508.
- Kilic F, Eskitascioglu T, Aydin A, et al., (2021): Ameliorating Effects of β -Glucan on Epigastric Artery Island Flap Ischemia-Reperfusion Injury. *Journal of Surgical Research*, 261:282-292. doi: 10.1016/j.jss.2020.12.035. Epub 2021 Jan 18. PMID: 33477077.
- Khan SU, Jannat S, Shaukat H, et al., (2023): Stress Induced Cortisol Release Depresses the Secretion of Testosterone in Patients with Type 2 Diabetes Mellitus. *Clinical Medicine Insights Endocrinology and Diabetes*, 3; 16:11795514221145841. doi: 10.1177/11795514221145841. PMID: 36636127; PMCID: PMC9830570.
- Khodamoradi K, Khosravizadeh Z, Amini-Khoei H, et al., (2020): The effects of maternal separation stress experienced by parents on male reproductive potential in the next generation. *Heliyon journal*, 6(9): e04807. doi: 10.1016/j.heliyon. 2020. e04807. PMID: 33024852; PMCID: PMC7527646.
- Kostenko, V.O., Shepitko, V.I. and Goltsev, A.N., (2019): Influence of the 30-days central deprivation of testosterone synthesis on the morphological and functional features of rat testicular interstitial endocrinocytes and sustentocytes. *Мир медицины и биологии journal*, 15(4 (70)), pp.228-233.
- Kue, J. (2007): *Electron microscopy methods and protocols*. New Jersey. Springer. Science & Business Media 3:1-8
- Liu H, Ding S, Nie H, et al., (2022): PM_{2.5} exposures at different concentrations and modes induces reproductive toxicity in male rats mediated by oxidative and endoplasmic reticulum stress. *Ecotoxicology Environmental Safety journal*, 244:114042. doi: 10.1016/j.ecoenv.2022.114042. Epub 2022 Sep 7. PMID: 36087467.
- Mokhtar HEL, Hulail MAE, Mahmoud SM, et al., (2021): Impact of cisplatin administration on cerebellar cortical structure and locomotor activity of infantile and juvenile albino rats: the role of oxidative stress. *Anatomical Science International journal*, 97(1):30-47. doi: 10.1007/s12565-021-00624-9. Epub 2021 Aug 13. PMID: 34386931.
- Nateghian, Z., Aliabadi, A. and Aliabadi, E., (2021): Effects of Stress-Induced Glucocorticoids on Reproductive Dysfunction in Men. *Journal of Advanced Biomedical Sciences*, 11(2), pp. 3780-3790.
- O'Kane SM, Mulhern MS, Pourshahidi LK, et al., (2018): Micronutrients, iodine status and concentrations of thyroid hormones: a systematic review. *Nutrition Reviews*, 76(6):418-431. doi: 10.1093/nutrit. /nuy008. PMID: 29596650.
- Pałkowska-Goździk E, Lachowicz K, and Rosołowska-Huszcz D. (2017): Effects of Dietary Protein on Thyroid Axis Activity. *Nutrients journal*, 10(1):5. doi: 10.3390/nu10010005. PMID: 29271877; PMCID: PMC5793233.
- Sawilowsky, S. (2005) Misconceptions leading to choosing the t test

- over the Wilcoxon Mann-Whitney U test for shift in location parameter. *Journal of Modern Applied Statistical Methods*, 4 (2): 598–600.
- Somade, O.T., Ajiboye, B.O., Osukoya, O.A., et al., (2023): Syringic acid ameliorates testicular oxidative stress via the conservation of endogenous antioxidant markers and inhibition of the activated Nrf2-Keap1-NQO1-HO1 signaling in methyl cellosolve-administered rats. *Pharmacological Research -Modern Chinese Medicine journal*, 6, p.100207.
- Son YL, Ubuka T and Tsutsui K. (2022): Regulation of stress response on the hypothalamic-pituitary-gonadal axis via gonadotropin-inhibitory hormone. *Frontiers in Neuroendocrinology journal*, 64:100953. doi: 10.1016/j.yfrne. 2021.100953. Epub 2021 Oct 29. PMID: 34757094.
- Suvarna KS, Layton C, Bancroft JD (eds) (2018): Bancroft's theory and practice of histological techniques. 8th ed. Elsevier, Amsterdam pp 25–130
- Thumfart KM, Lazzeri S, Manuella F, et al., (2022): Long-term effects of early postnatal stress on Sertoli cells. *Frontiers in Genetics*, 13:1024805. doi: 10.3389/fgene.2022.1024805. PMID: 36353105; PMCID: PMC9638847.
- Wang R, Huang Y, Yu L, et al., (2023): The role of mitochondrial dynamics imbalance in hexavalent chromium-induced apoptosis and autophagy in rat testis. *Chemico- Biological Interactions journal*, 374: 110424. doi: 10.1016/j.cbi. 2023. 110424. Epub 2023 Feb 26. PMID: 36849043.
- Widström AM, Brimdyr K, Svensson K, et al., (2019): Skin-to-skin contact the first hour after birth, underlying implications and clinical practice. *Acta Paediatrica journal*, 108(7): 1192-1204. doi: 10.1111/apa. 14754. Epub 2019 Mar 13. PMID: 30762247; PMCID: PMC6949952.